ANALYSIS OF LIGHT WATER REACTORS INCLUDING 3-D DETERMINISTIC BURNUP OF A BOILING WATER REACTOR FUEL ASSEMBLY

By

MIREILLE ANJALINE ROWE

A THESIS PRESENTED TO THE GRADUATE SCHOOL
OF THE UNIVERSITY OF FLORIDA IN PARTIAL FULFILLMENT
OF THE REQUIREMENTS FOR THE DEGREE OF
MASTER OF SCIENCE

UNIVERSITY OF FLORIDA

2009

To Ricardo A. Cortes Jr. and my parents, Mireya and Franklin Sotillo and Tomas Rowe

ACKNOWLEDGMENTS

I would like to thank my advisor Dr. Glenn Sjoden for providing technical guidance throughout my research and for always being available for help and advice. I also wish to acknowledge Kevin Manalo, Travis Mock and Thomas Plower for their contribution in the PENTRAN/PENBURN suite and helping with adapting the code package for use in analyzing BWR's. And I would also like to thank my thesis committee members Dr. Edward Dugan and Dr. Robert Smith.

TABLE OF CONTENTS

LIST OF TABLES

LIST OF FIGURES

LIST OF ABBREVIATIONS

ALPO	ANISN library production option
BONAMI	Bondarenko AMPX interpolator
BWR	Boiling Water Reactor
CENTRM	Continuous energy transport module
GMIX	Generalized cross section mixer
MCNP	Monte Carlo neutral particle transport code
NEWT	New extended step characteristic-based transport code
PENBURN	Parallel environment burnup
PENTRAN	Parallel environment neutral particle transport
PMC	Produce multigroup cross sections
SCALE	Standardized computer analysis for licensing evaluation
SFCOMPO	Spent fuel isotopic composition database
TRITON	Transport rigor implemented with quasi-static time dependent operation for neutronic depletion

Abstract of Thesis Presented to the Graduate School
of the University of Florida in Partial Fulfillment of the
Requirements for the Degree of Master of Science

ANALYSIS OF LIGHT WATER REACTORS INCLUDING 3-D DETERMINISTIC BURNUP OF A BOILING WATER REACTOR FUEL ASSEMBLY

By

Mireille Anjaline Rowe

August 2009

Chair: Glenn Sjoden
Major: Nuclear Engineering Sciences

Accurate transport analysis of reactor systems is important in the Nuclear Engineering field since it provides essential information in power monitoring, criticality safety and fuel reload optimization. Monte Carlo methods have primarily been used to analyze these reactor systems, yet drawbacks include difficulty converging the source in an eigenvalue problem when dealing with high dominance ratio systems (Brown, et. al., 2003). Deterministic 3-D Sn transport computations have been utilized in limited ways due to the large memory requirements of these methods. For this reason, 1-D or 2-D geometry set-ups are usually implemented, and important information regarding the system may be lost as is the case with boiling water reactors (BWRs). In order to evaluate a 3-D model of a system with a deterministic transport code, one that runs in parallel can provide unique advantages. This thesis presents a method to generate a multigroup cross section data set and transport models for analysis of reactors. Next an analysis of a light water reactor system using the 3-D parallel code PENTRAN (Parallel Environment Neutral particle Transport) to perform adjoint transport calculations and provide information on effective detector ranges in PWRs is discussed. In addition, a detailed fuel burnup analysis of a BWR using the PENTRAN/PENBURN (Parallel Environment Burnup) suite is presented.

CHAPTER 1
INTRODUCTION

1.1 Introduction

Radiation analysis of large power reactors is rarely performed using 3-D deterministic transport techniques. Reaction rates and flux calculations for burnup analysis are usually evaluated using 3-D nodal diffusion theory and 2-D transport theory approximations. This leaves an unsatisfied technical need for burnup validation in a 3-D environment simulation.

PENTRAN has proved to be a time efficient algorithm for solving the Linear Boltzmann Transport equation in a heterogeneous 3-D environment. PENBURN was developed in order to process 3-D neutron flux distributions from PENTRAN and calculate reaction rates for 3-D burnup analysis. The body of this work contains the method of multigroup cross section generation, calculation of detector response, analysis of a 6x6 BWR assembly, full 3-D reactor flux, and burnup distributions in comparison with post irradiation experiments from SFCOMPO.

1.2 Transport Theory

The distribution of neutrons in a given nuclear reactor system can be characterized by linear Boltzmann equation (LBE) similar to the equation governing the kinetic theory of gases. The integro-differential form of the neutron transport equation is given in the following equation:

$$\frac{1}{v}\frac{\partial\psi(\vec{r},E,\hat{\Omega},t)}{\partial t}+\hat{\Omega}\cdot\nabla\psi\left(\vec{r},E,\hat{\Omega},t\right)+\sigma(\vec{r},E)\psi\left(\vec{r},E,\hat{\Omega},t\right)$$

$$=\int_0^\infty dE'\int_{4\pi}d\hat{\Omega}'\,\sigma_s\left(\vec{r},E'\rightarrow E,\hat{\Omega}\rightarrow\Omega\right)\psi\left(\vec{r},E',\hat{\Omega}',t\right)$$

$$+\frac{\chi(E)}{4\pi}\int_0^\infty dE'\int_{4\pi}d\hat{\Omega}'\,\nu(E')\sigma_f(\vec{r},E')\psi\left(\vec{r},E,\hat{\Omega}',t\right)+q_{ext}\left(\vec{r},E,\hat{\Omega},t\right) \qquad (1\text{-}1)$$

Where v = neutron speed
ψ = neutron particle flux
$\vec{r}$ = neutron location in space

E = neutron energy
$\hat{\Omega}$ = direction of unit vector
t = time
σ = total macroscopic cross section
σ_s = differential scattering cross section
χ = fission spectrum
ν = average number of fission neutrons produced per fission
σ_f = fission cross section
q_{ext} = external neutron source

The left hand side of this equation includes the losses in the system due to leakage and collision, while the right hand sign includes the production in the system from scatter, fission and any independent external sources. In all, there are seven independent variables in the neutron transport equation, along with a strong cross section dependence on energy, which results in a complex and difficult equation to solve, even with the use of computers. For this reason, diffusion theory is sometimes used instead of the neutron transport equation (Lewis and Miller, 1993).

1.3 Diffusion Theory

The diffusion approximation considers the neutron flux as a function of space, energy and time. In order to obtain this, the neutron transport equation is integrated term by term over all directions resulting in the zeroeth angular moment balance equation. The first angular moment is then introduced to provide two equations with two unknowns: flux and current. Assuming the angular flux depends weakly on angle, the set of P_1 equations are derived as shown in equations 1-2 and 1-3.

$$\frac{1}{v}\frac{\partial\varphi(\vec{r},t)}{\partial t} + \nabla\cdot\vec{J}(\vec{r},t) + \sigma(\vec{r},E)\varphi(\vec{r},t) = \sigma_s(\vec{r})\varphi(\vec{r},t) + \nu\sigma_f(\vec{r})\varphi(\vec{r},t) + q_{ext}(\vec{r},t) \quad (1\text{-}2)$$

$$\frac{1}{v}\frac{\partial\vec{J}(\vec{r},t)}{\partial t} + \frac{1}{3}\nabla\varphi(\vec{r},t) + \sigma(\vec{r})\vec{J}(\vec{r},t) = \sigma_{s1}(\vec{r})\vec{J}(\vec{r},t) + q_{ext\,1}(\vec{r},t) \quad (1\text{-}3)$$

Additional approximations include considering only isotropic sources, and that the time derivative in current can be neglected in comparison with the other terms in the equations. An approximation for the current is subsequently obtained, as shown in Equation 1-4, and the diffusion constant is determined, as noted in Equation 1-5.

$$\vec{J}(\vec{r},t) = -\frac{1}{3(\sigma-\sigma_{s1})}\nabla\varphi(\vec{r},t) \tag{1-4}$$

$$D = \frac{1}{3(\sigma-\sigma_{s1})} \tag{1-5}$$

The P_1 equations can then be simplified by substituting the diffusion constant into equation 1-2 to obtain the one speed diffusion equation as shown below.

$$\frac{1}{v}\frac{\partial\varphi(\vec{r},t)}{\partial t} - D\nabla^2\varphi(\vec{r},t) + \sigma(\vec{r},E)\varphi(\vec{r},t) = \sigma_s(\vec{r})\varphi(\vec{r},t) + \nu\sigma_f(\vec{r})\varphi(\vec{r},t) \tag{1-6}$$

Recalling the different assumptions that were made in order to arrive at the diffusion equation, it is evident that there are significant limitations that should be considered when using the diffusion approximation. Instances when the diffusion approximation is not valid include when the angular flux is highly dependent on angle. Certain cases where this approximation is not valid include regions where the neutron flux varies drastically over short distances compared to the neutron mean free path, interfaces between dense materials, and a vacuum, close to external neutron sources, materials with high absorption cross sections such as control rods, or materials that have a strong anisotropic scattering cross section (Duderstadt and Hamilton, 1976).

1.4 Monte Carlo Method

The Monte Carlo method uses a series of random events to simulate a physical process. This statistical method uses random numbers generated from a computer to determine an average value for a physical process by means of random sampling of probability distribution functions (Kalos and Whitlock, 1986). In nuclear engineering, this technique has been used for reactor

shielding and criticality and dose calculations. Although it has been widely used for particle transport simulations, it does contain drawbacks, including the large computational time required to sample sufficiently from a certain regions to obtain reliable results, as well as experiencing false source convergence when dealing with eigenvalue problems (Haghighat and Wagner, 2003).

1.5 Deterministic Code: PENTRAN/PENBURN Suite

The PENTRAN/PENBURN Suite was used primarily for this work. PENTRAN is a 3-D transport solver that can be run in parallel with angle, group and spatial decomposition (Sjoden and Haghighat, 2008). It solves the 3-D multigroup steady state form of the LBE as shown in Equation 1-7 by averaging over the energy groups from high to low energies.

$$\hat{\Omega}\cdot\nabla\psi_g(\vec{r},\hat{\Omega})+\sigma_g(\vec{r})\psi_g(\vec{r},\hat{\Omega})=$$

$$\sum_{g'=1}^{g}\int_{4\pi}d\Omega'\sigma_{s\,g'\to g}(\vec{r},\hat{\Omega}'\cdot\hat{\Omega})\psi_{g'}(\vec{r},\hat{\Omega}')+\frac{\chi_g}{k_o}\sum_{g'=1}^{G}\int_{4\pi}d\Omega'\nu\sigma_{f\,g'}(\vec{r})\psi_{g'}(\vec{r},\hat{\Omega})+q_{ind\,g}(\vec{r},\hat{\Omega}) \qquad (1\text{-}7)$$

PENBURN is a coupled fuel depletion solver that, when provided with reaction rates, computes the time-dependent isotope concentrations using the direct Bateman solution for a set of about 150 actinides and fission products (Manalo, 2008). The path matrix keeps track of the linear chain that the actinides and fission products undergo, and the Bateman batch equation in Equation 1-8 provides the solution for the nuclide concentrations.

$$N_i(t)=\sum_{l=1}^{i-1}\left(N_l^o\eta_l\eta_{l-1}\ldots\eta_{i-1}\sum_{j=1}^{i}\frac{e^{-\mu_j t}}{\prod_{\substack{k=l\\k\neq j}}^{i}\left(\mu_k-\mu_j\right)}\right)+N_i^o e^{-\mu_i t} \qquad (1\text{-}8)$$

Where N_l = number of atoms of precursor nuclide l at time t=0
η_l = the chain-linking precursor rate constant
μ_i = the effective decay constant for nuclide I, accounting for $\sum_{g=1}^{G}\sigma_g\,\varphi_g$ and λ

$N_i(t)$= the number of atoms of nuclide i at time t
N_i^0 = the number of atoms of nuclide I at time t=0

A useful feature is the availability to modify the path matrix to add additional actinides of interest if the user would like to track more nuclides.

1.6 Previous Work

Significant work on burnup in BWR systems has been performed in 2-D; by comparison, less research has been published with regard to computing full 3-D burnup analysis of boiling water reactor fuel assemblies (DeHart and Hermann, 1998. Limitations have included computational time and memory requirements. Burnup code developers have however used SFCOMPO post irradiation examination data from fuel removed from reactors as a way to validate their code results. The SFCOMPO database provides the isotopic composition of spent fuel from light water reactors and operating parameters including initial fuel enrichment, burnup, and axial location of the fuel pellet sample analyzed. There is a lack of information however regarding control rod positioning and moderator density at different core heights which experience has shown greatly affects fuel discharge isotopics and fission product content. The SFCOMPO database also contains fuel assembly designs that are different from more recent BWRs including the uniform enrichment of the fuel axially, and the lack of water holes in the assembly.

1.6.1 SCALE SAS2H BWR Burnup Analysis

The SAS2H sequence in SCALE uses transport methods along with depletion and decay from ORIGEN-S to determine the isotopic composition of fuel after a set burnup level. It had previously been used to compare with SFCOMPO data available for BWR assemblies. The transport code XSDRNPM used in SCALE is 1-D and therefore simplifications were necessary to model the BWR. A set of rings with the fuel, clad and moderator was modeled while still

preserving material mass. Although multiple fuel pin data was available for different axial heights in the assembly, an average of the final fuel composition was computed before comparing to the burnup results from SCALE. The report indicated agreement with SFCOMPO for a majority of the actinide results to within 32%. Since all of the fuel was essentially lumped together, it was not a direct comparison with SFCOMPO data which provides specific pin isotopic compositions (DeHart and Hermann, 1998).

1.6.2 Void Fraction Uncertainties

Studies have been conducted to determine the effect that void uncertainties have even initially during startup due to absorber blade insertions, utilizing different cross section data libraries and water films created within bundles. The study was performed when analyzing a 10 x 10 BWR Westinghouse fuel assembly and utilizing different data libraries resulted in a 40% differences between void predictions. Accounting for water films within channels accounted for a 4% difference in pin powers and insertion of control blades contributed to a change of 10% in pin power values (Jatuff, F., et. al., 2005).

CHAPTER 2
MULTIGROUP CROSS SECTION GENERATION

Developing accurate cross section data sets is important in order to model the physics correctly for any reactor system. The deterministic code used in these analyses requires the user to provide multigroup cross section data for the reactor systems being analyzed. This section will describe the procedure used to acquire the multigroup cross section data from the SCALE 5.1 package, in addition to demonstrating how to generate multiple cross section data for the same nuclide as it applies to different void fractions for the BWR problem.

2.1 Cross Section Generation with SCALE 5.1 Package using DEV-XS Procedure

SCALE is a modular code system which uses automated sequences that can provide information on cross section processing, reactor physics, criticality safety, radiation shielding, and spent fuel and high level waste characterization. For reactor physics applications the TRITON control module is utilized in addition to the functional module NEWT. TRITON is a SCALE control sequence that calls NEWT to perform the transport physics analysis for a specified 2-D configuration.

The SCALE 5.1 package was primarily used to generate the multigroup cross section data for the reactor systems analyzed following the DEV-XS procedure, a cross section development primer for the PENTRAN/PENBURN suite. Figure 2-1 displays the flow path for the cross section development used when following the DEV-XS procedure (Plower, 2008).

2.1.1 SCALE 5.1 TNEWT Control Sequence

The t-newt driver for the transport calculation was used, which executes NEWT transport calculations using cross sections prepared within the sequence. The sequence includes the self-shielding modules: BONAMI, WORKER, CENTRM and PMC.

The BONAMI module is the unresolved resonance self-shielding processor which uses the Bondarenko method (Greene, 2006). CENTRM creates the space dependent (1-D), point wise continuous energy flux file (Asgari et al, 2006). PMC creates a problem-dependent master library from the CENTRM flux spectrum (Hollenbach and Williams, 2006). Finally, the WORKER module creates working libraries from the master libraries (Hollenbach and Petrie, 2006). A sample SCALE 5.1 input file is found in Appendix A.

2.1.2 Post-Processing Utilities

In addition to using the TNEWT control sequence, three utilities are used to create inputs needed for GMIX, which creates the macroscopic data set used by PENTRAN. The SCALFORM utility converts cross section file generated using the SCALE5.1 ALPO module into a standard ASCII format file used by PENTRAN. The user indicates the name of the cross section input file, number of energy groups, number of columns of data, the column position for σ_t, and the column position number in which all scattering cross section values are nonzero. The output file created by SCALFORM contains all of the microscopic cross section data.

The Perl script GMIXFORM uses the initial SCALE 5.1 input file to create a GMIX input file that contains the material composition information and cross section formatting data. The Perl script COLLAPSEFORM uses the initial SCALE 5.1 input file to create the file with neutron energy group structure and primary neutron fission temperature.

2.1.3 GMIX Code

The previous section discussed how to generate the three input files required by GMIX: .xsc, .gmx, and .grp files. Once these files are generated, the user modifies the .gmx input file to include the microscopic cross section input filename, the data path location, the output filename, the number of energy groups, column information and the P_n order. The GMIX code blends the

cross section data into macroscopic material cross section data used by PENTRAN (.xs file) and also outputs the .chi file containing the normalized fission spectrum data.

2.2 BWR 2.2 wt% Fuel Pin Cross Section Generation

Some preliminary analysis on a unit pin cell was performed in order to gain useful information for the full 3-D reactor model. The pin selected for this study is a UO_2, 2.2% enriched BWR-6 fuel element. The composition of the fuel pin clad was chosen as natural zirconium with a density of 6.508 g/cm^3 and a temperature of 577 K, while the fill gas was helium with a density of 0.07518 g/cm^3. The core had a specified operating pressure of 7.17 MPa.

SCALE 5.1 was used to generate group flux weighted multigroup cross sections for a 2-D unit cell. The cross sections were used to validate eigenvalue calculations between SCALE5.1 and PENTRAN. Material balance approximations for the Cartesian hexahedral geometry in PENTRAN were also considered.

P_1 cross sections were developed using SCALE 5.1 and the DEV-XS process developed for blending group flux weighted cross sections in the specified materials for use in PENTRAN. The 238 group ENDF/B-VI library was collapsed to 3 groups with upper MeV bounds of 20.0 MeV, 1.0 MeV, and 0.625 eV, respectively to match the energy group structure in the ORIGEN-S depletion module from SCALE 5.1.

As a result of using a Cartesian geometry in PENTRAN, it was important to validate material balance on eigenvalue results. The amount of excess fissile material was particularly of concern for eigenvalue comparisons. Table 2-3 displays the eigenvalue comparisons between SCALE 5.1 and meshing associated with excess fissile material values. After examining the results it was apparent that a 19 x 19 meshing scheme for each pin cell provides the most physically accurate results, while still reasonably representing the amount of fissile material.

2.3 XSMERGE Code

Certain problem set-ups use multiple regions of the same material while utilizing varied microscopic cross sections as is the case with the BWR. In order to generate the cross sections necessary for PENTRAN, the DEV-XS procedure is followed for each configuration which results in multiple microscopic cross section files. Each of the microscopic cross section files has to be combined into one file and sorted by nuclide in order for GMIX to process it. The XSMERGE code was developed to combine and sort multiple microscopic cross section files generated by the user.

The XSMERGE code combines each microscopic cross section file generated by the user, groups them according to nuclide, and sorts the nuclide lists in ascending order based on the SCALE 5.1 material number previously assigned. The output file generated by XSMERGE is now in a usable format that GMIX can process to create the macroscopic cross sections that PENTRAN directly utilizes. This ensures the correct cross sections are used in each of the regions of the problem.

In order to run XSMERGE, the user specifies the input file name that will contain the number of files to sort, the microscopic cross section file names, and the output file name. The flow path for the cross section development utilizing XSMERGE is displayed in Figure 2-2.

A sample problem to display the use of the XSMERGE code was developed and deals with a single BWR pin containing two different water densities as shown in Figure 2-3. The DEV-XS procedure was followed twice for each pin, the first with a moderator density of 0.75574 g/cm^3 corresponding to the core height within the non-boiling length of 154 cm and the second with a moderator density of 0.72055 g/cm^{3}corresponding to a core height of 157 cm. Table 2-4 demonstrates the material numbers used in the SCALE 5.1 input and Figure 2-1 displays the BWR pin model with the appropriate SCALE5.1 material numbers used. The microscopic cross

section files (water1.xsc and water2.xsc) generated after running the first and second SCALE 5.1 inputs are merged together using the XSMERGE program and results in the combined and sorted microscopic cross section file (bwrpin.xsc).

The following displays the sample input needed to run XSMERGE:

```
                    XSMERGE
 SCALFORM Cross Section file (.xsc) sorter
 G. Sjoden, K. Manalo, T. Plower, M. Rowe


 Enter input file name
xmerge.inp
```

Below is an example of the sample input file:

```
/No of files to process
2
/xsc file names
water1.xsc
water2.xsc
/output file name
bwrpin.xsc
```

Table 2-1. BWR/6 fuel assembly specifications

Thermal Output	3579 MW(t)
Active Height	375.92 cm
Number of Fuel Assemblies	732
Fuel Element Array	8 x 8
Assembly Dimensions	14.02 cm x 14.02 cm
Assembly Pitch	15.24 cm
Number of Fuel Rods/Assembly	62
Total Number of Fuel Rods	45,384
Fuel Rod O.D.	1.25222 cm
Fuel Rod Pitch	1.6256 cm
Pitch/Diameter	1.3
Clad Thickness	0.08636 cm
Fuel Pellet Diameter	1.05664 cm
Pellet-Clad Gap	0.01143 cm
Fuel Enrichment	2.2-2.7%
System Pressure	7.17 MPa
Average Exit Quality	14.6%
Core Average Void Fraction	42.6%
Maximum Exit Void Fraction	76%
Core Inlet Temperature	532 F
Outlet Temperature	547 F

Table 2-2. BWR/6 2.2 wt% fuel pin composition

Nuclide	Wt%
O^{16}	11.8502
U^{234}	0.0224
U^{235}	1.9393
U^{236}	0.0122
U^{238}	86.17424
Total	100

Table 2-3. Eigenvalue comparisons for PENTRAN unit cell meshing schemes

Eigenvalue (PENTRAN)	% difference from SCALE 5.1 (1.185)	% excess fissile material	Meshing
1.191	0.506	2.8	15 x 17
1.182	-0.253	1	19 x 19
1.200	1.266	0.8	23 x 23

Table 2-4. XSMERGE example problem material numbers assigned.

Material #'s in SCALE5.1 Input		
Scale Input	1	2
Density (g/cc)	0.75574	0.72055
Fuel	11	12
Gap	21	22
Clad	31	32
H_2O	41	42

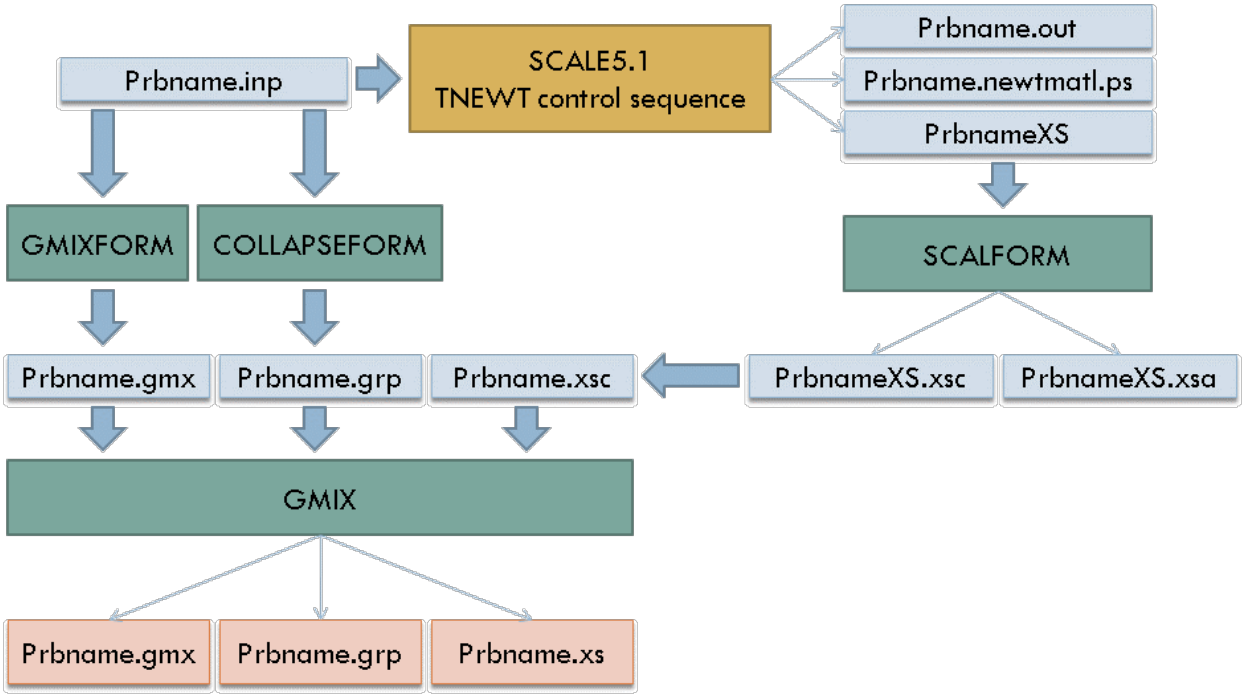

Figure 2-1. Flow path of cross section development.

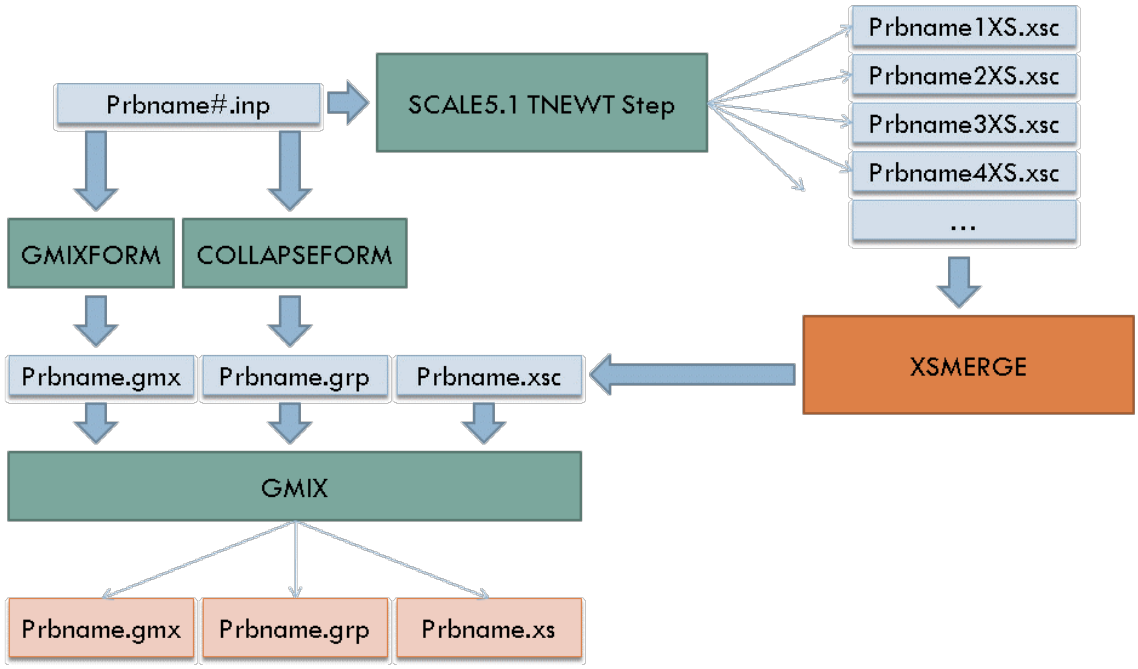

Figure 2-2. Flow path of cross section development for BWR.

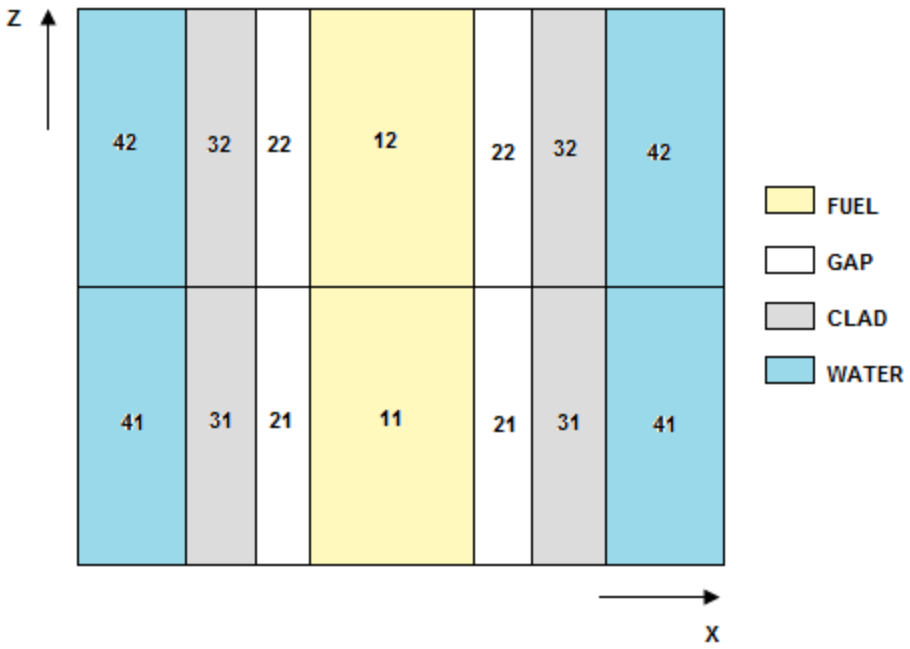

Figure 2-3. XSMERGE example problem model with corresponding material numbers.

CHAPTER 3
AN APPLICATION OF FORWARD AND ADJOINT TRANSPORT

Evaluation of silicon carbide (SiC) semiconductor detectors for use in power monitoring is of interest because of their distinct advantages, including small size, small mass, and their inactivity both chemically and neutronically. The main focus of this section is in evaluating the predicted response of a SiC detector when placed in a 17x17 Westinghouse PWR assembly. Transport computations were performed using the PENTRAN (Parallel Environment Neutral-particle Transport) code system for the 3-D deterministic adjoint transport computations. Adjoint transport results enable one to assess the relative spectral contributions of a source in causing a signal in a detector, and can therefore be used to evaluate the effective detector range. Subsequent sections in this chapter will include a description of the detector model, multi-group cross-sections, description of the forward and adjoint transport response calculations, and results. Included is a discussion of the relative influence (as determined by the adjoint results) of fuel pins to the SiC neutron detector response based on pin radial proximity to the detector.

3.1 Silicon Carbide Detector Design

Silicon carbide detectors have been proposed primarily by Westinghouse for power monitoring purposes in PWRs. The silicon carbide detector design considered in this paper is based on a design with material layers including 300 μm 4H-SiC substrate, 1 μm Au, 8 μm Al, and 1μm enriched LiF (Khorsandi, et. al. 2006). The neutron response in the detector is produced by the neutrons penetrating the SiC; fast and epithermal neutrons interact directly with the SiC to form energetic reaction products capable of producing ionization events in the detector (Dulloo et. al, 2003). Also, after penetrating the SiC, neutrons can interact with the thin lithium layer to produce alpha and triton reaction products. The aluminum layer is placed in between the LiF and Au layers in order to minimize radiation damage effects from the alpha particles. The

triton particles pass through the aluminum foil and are deposited in the inactive SiC substrate layer. Previous analysis shows that SiC detectors withstand a fast neutron irradiation fluence of 3.4×10^{17} cm^{-2} and are designed to work at high temperatures (Ruddy, et. al., 2006). For the purposes of this study, the SiC detector was modeled as a homogenized material of LiF, Al, Au and primarily SiC with a density of 3.2 g/cm^3.

3.2 Multi-group Cross Section Generation

Three group cross sections ($E_3 < 0.625$ eV; 0.625 eV $< E_2 <$ 1.01 MeV; $E_1 >$ 20 MeV) were developed using SCALE 5.1's T-NEWT control sequence by collapsing the 238 group ENDF-B-VI AMPX library as discussed in the previous chapter. A lattice cell calculation was performed for a homogenized 3 wt% enriched PWR fuel pin, and the SiC detector was modeled as a homogenized, density scaled mesh cell comprised of LiF, Al, Au and SiC. The nuclide composition of the 3 wt% enriched UO_2 fuel is shown in Table 1. The density of the water was 0.6612 g/cm^3, based on an operating pressure of 15.2 MPa and an operating temperature of 600K. A thin layer (thickness=0.22 μm) of the homogenized silicon carbide was placed around the homogenized PWR fuel pin. For the SCALE 5.1 NEWT flux calculations (S_8), a convergence value of $5x10^{-5}$ was chosen for the spatial and eigenvalue iterations. Mirror reflection albedo conditions were chosen for the external boundaries of the unit cell. The k_{eff} results for the homogenized PWR pin (fuel and cladding) compared to that of the homogenized PWR with the SiC detector placed nearby it displayed a difference of 0.3% Δk, indicating the impact the presence of the SiC detector has neutronically to the lattice.

3.3 Forward versus Adjoint Detector Response

The steady state multi-group form of the transport equation operating on the forward group angular flux ψ_g is [5]:

$$\hat{\Omega}\cdot\nabla\psi_g(\vec{r},\hat{\Omega})+\sigma_g(\vec{r})\psi_g(\vec{r},\hat{\Omega})=\sum_{g'=1}^{G}\int_{4\pi}d\Omega'\,\sigma_{s\,g'\to g}(\vec{r},\hat{\Omega}'\cdot\hat{\Omega})\,\psi_g(\vec{r},\hat{\Omega}')+q_g(\vec{r},\hat{\Omega}) \quad (3\text{-}1)$$

Principally, scattering comes from all other groups *g'* into group *g*. is dominated by down-scattering from higher energies to lower energies. The adjoint transport operator H^+ can be derived using the adjoint identity for real valued functions, and the forward multi-group transport operator, where $\langle\ \rangle$ represents integration over all independent variables:

$$\left\langle \psi_g^+\ H\,\psi_g \right\rangle = \left\langle \psi_g\ H^+\psi_g^+ \right\rangle \quad (3\text{-}2)$$

Using Equation 3-1, it can be seen that the forward operator is

$$H=\hat{\Omega}\cdot\nabla+\sigma_g(\vec{r})-\sum_{g'=1}^{G}\int_{4\pi}d\Omega'\,\sigma_{s\,g'\to g}(\vec{r},\hat{\Omega}'\cdot\hat{\Omega}) \quad (3\text{-}3)$$

The angular adjoint (importance) function is ψ_g^+. Applying the adjoint boundary condition that particles leaving a bounded system have an importance of zero in all groups (converse of the forward vacuum boundary condition) with the above equations, and requiring a continuous importance function mathematically leads to the multi-group adjoint transport operator:

$$H^+=-\hat{\Omega}\cdot\nabla+\sigma_g(\vec{r})-\sum_{g'=1}^{G}\int_{4\pi}d\Omega'\,\sigma_{s\,g\to g'}(\vec{r},\hat{\Omega}\cdot\hat{\Omega}') \quad (3\text{-}4)$$

Note the minus sign on the streaming term indicates that adjoint particles travel along a 'reversed' direction, where adjoint scattering progresses from group *g back* to other groups *g'*

(those groups formerly contributing *to* group *g* in the *forward* equation). The forward neutron detector fixed source response can be solved by satisfying the transport equation

$$H\psi_g = q_g \tag{3-5}$$

and the adjoint transport equation can be satisfied using an adjoint source that is aliased to the group detector response cross section σ_{dg}:

$$H^{+}\psi_g^{+} = \sigma_{d\,\mathrm{g}} \tag{3-6}$$

Applying Equations 3-2, 3-5, and 3-6, and integrating over all variables results in the useful expression for detector response *R*:

$$R = \left\langle \psi_g \sigma_{d\,\mathrm{g}} \right\rangle = \left\langle \psi_g^{+} q_g \right\rangle \tag{3-7}$$

From Equation 3-7, it is clear that, detector response can be obtained by complete integration of the source distribution with the adjoint function—for any arbitrary source distribution. Therefore, *R* can be computed directly from the results of either of *several* forward transport computations for each neutron source distributions, or one single adjoint transport computation with coupling to each source density distribution.

Therefore, the silicon carbide detector response can be calculated by summing the product of the neutron flux, detector cross section, and cell volume for all groups and all meshes that contain the detector, as indicated in Equation 3-8 (Sjoden, 2002).

$$\sum_{\substack{\Delta V_i \epsilon V_d \\ g=1,G}} \varphi_{g,i} \sigma_{d\,g,i} \Delta V_i \tag{3-8}$$

Similarly, the adjoint transport response is determined by summing the product of the adjoint function, neutron source, and cell volume for all groups and all meshes as displayed in Equation 3-9.

$$\sum_{\substack{\Delta V_i \epsilon V_d \\ g=1,G}} \varphi_{d\ g,i}^{+} q_{g,i} \Delta V_i \tag{3-9}$$

3.4 PENTRAN Criticality Calculation

A quarter model of a 17x17 Westinghouse OFA assembly with the SiC detector placed in the center location of the assembly and a transport calculation was performed with PENTRAN as illustrated in Figure 3-1. The dimensions of the quarter assembly were 0.0 cm to 10.75 cm in the x and y axes, and an axial height of 17 cm, with a geometry consisting of 48 coarse meshes. The SiC detector location resided in coarse mesh 32 (top right corner) with its center at a z-level of 8.5 cm, occupying a total of 3 fine meshes. The density of the SiC detector material was decreased to 0.022864 g/cm^3 accordingly to preserve mass. The multi-group cross-sections developed from the homogenized fuel and homogenized SiC unit cell model were used for the quarter assembly. The angular quadrature was set to S_8 with an inner flux tolerance of $1x10^{-4}$ and outer criticality tolerance of $1x10^{-5}$. Reflective boundary conditions were set for all outer boundaries of the model. The k_{eff} value was 1.31525, with a tolerance of 2.72×10^{-6}.

Based on a criticality calculation, a fixed source calculation was performed with PENTRAN. The fixed source calculation was scaled according to the relative number of particles from the criticality run. A post processing code, FSPREP, was developed to render the fixed fission source distribution based on the criticality calculation output; this was used to set up the source in the fuel for a fixed source calculation. The total source from both runs is in good agreement, as shown in Tables 2 and 3. The balance shown in these tables is an absolute particle balance.

3.5 FSPREP Code

The FSPREP code extracts the fission source results from an initial criticality run and outputs the fine mesh spatial distribution for the coarse mesh source. The input file required by FSPREP contains the number of energy groups in the model, the source file names for each energy group, the number of coarse meshes that contain the source, and the reference location of the sources in order of source number by coarse mesh number. A sample input file is shown in Appendix B. The source files for each energy group should use the format of: coarse number, mesh number, material number, x location, y location, z location and source value. The resulting output file contains the *spacpf* variable for Block 5 of the PENTRAN input deck. This variable indicates the source number, group number, number of sequentially numbered meshes, and corresponding mesh spatial probabilities only for the sources that require a non-uniform spatial probability distribution. Figure 3-2 displays the flow path taken when utilizing the FSPREP code. Appendix C contains an excerpt of a sample output file generated by FSPREP.

3.6 PENTRAN Adjoint Calculation

The PENTRAN forward transport solver can be utilized to solve for the adjoint function with the detector cross section as the adjoint source. This is performed by transposing (reversing) group cross sections, sources, and the scattering matrix. The forward cross sections are automatically reversed internally by the code, while sources are reversed by the user in the energy group probability distribution card. Group *G* is reported as Group 1, and subsequently Group 1 is reported as Group *G* for PENTRAN adjoint results. The tolerances set for the adjoint run were $1x10^{-4}$ for the inner convergence criteria.

3.7 Results and Findings

The adjoint function results by energy group are displayed in the following figures at a z-level of 9 cm. Each of the adjoint values represents the local neutron importance relative to the

response in the SiC detector. The maximum relative adjoint values for the thermal, epithermal and fast energy groups are 1, 0.507, and 0.308 respectively. The thermal group adjoint function values decrease rapidly as the radial distance from the semiconductor location increases. The importance relative to a thermal neutron causing a reaction in SiC drops by three orders of magnitude in moving more than 2 fuel pins away from the detector. Alternatively, in the epithermal and fast energy groups, the adjoint importance drops by three orders of magnitude after a radial distance of five fuel pins from the detector location.

The response of the detector is calculated from the forward transport computations with Equation 3-8 by summing the product of the neutron flux, the absorption cross section of the detector, and the cell volume of the meshes containing SiC over all the energy groups. The total cell volume of the SiC detector was 0.008 cm^3, and the forward neutron source was 4880 n/cm^3-s. The response of the detector is alternatively calculated from a single adjoint transport computation using Equation 3-9 and summing the product of the local adjoint function, cell fission source density, and cell volume over all energy groups. The total predicted neutron response from the forward calculation was 1.724×10^{-4} per second, and from the adjoint calculation the detector response was 1.654×10^{-4} neutrons (counts) per second. The differences between the two values can be attributed to the relative convergence and to some truncation error causing differences between the forward and the adjoint. The fuel pins within the inner circle shown in Figure 3-3 (at a radial distance of 6.08 cm) contribute to 75.33% of the neutron response from the thermal group. Similarly, 35.85% of the neutron response from the epithermal group comes from fuel in this radius, as does 21.58% from fast group contributions to neutron response. The relative fractions of the thermal, epithermal, and fast group to the overall neutron response were 72%, 27% and 1% respectively.

This work demonstrates the application of adjoint transport methods to determine the predicted response of a SiC detector when placed in a 17x17 Westinghouse PWR assembly. A single adjoint transport computation can be used to calculate the response of the detector, and can be utilized for different source terms, as opposed to performing several forward transport computations when dealing with varied sources. The adjoint results display the relative neutron importance by energy group, with the thermal group reporting the highest adjoint value for the SiC detector. For neutrons, the effective monitoring range of the SiC detectors is on the order of five PWR fuel pins away from the detector; pins outside this range in the fuel lattice are minimally "seen" by the SiC detector. Similar calculations can be performed for different detector designs to evaluate the use of SiC detectors in different systems.

Table 3-1. Nuclide composition of 3 wt% enriched UO_2 fuel

Nuclide	Wt%
O^{16}	11.8532
U^{234}	0.0224
U^{235}	2.6444
U^{236}	0.0122
U^{238}	85.4678
Total	100

Table 3-2. Integral System Balance from Criticality Run

Group	Leakage	Collisions	ScatterSrc	FissionSrc	Vol&BdySrc	Balance
1	9.69E-03	-1.00E+04	6.67E+03	3.38E+03	0.00E+00	-9.36E-02
2	7.44E-02	-9.07E+04	8.92E+04	1.49E+03	0.00E+00	8.97E-01
3	4.80E-03	-5.43E+04	5.43E+04	1.04E-06	0.00E+00	-2.65E-02
Total	8.89E-02	-1.55E+05	1.50E+05	4.88E+03	0.00E+00	7.77E-01

Table 3-3. Integral System Balance from Fixed Source Run

Group	Leakage	Collisions	ScatterSrc	FissionSrc	Vol&BdySrc	Balance
1	-4.56E-03	-1.00E+04	6.66E+03	0.00E+00	3.38E+03	3.04E-02
2	1.57E-03	-9.06E+04	8.91E+04	0.00E+00	1.49E+03	2.24E-02
3	7.82E-03	-5.43E+04	5.43E+04	0.00E+00	1.04E-06	2.74E-02
Total	4.83E-03	-1.55E+05	1.50E+05	0.00E+00	4.88E+03	8.02E-02

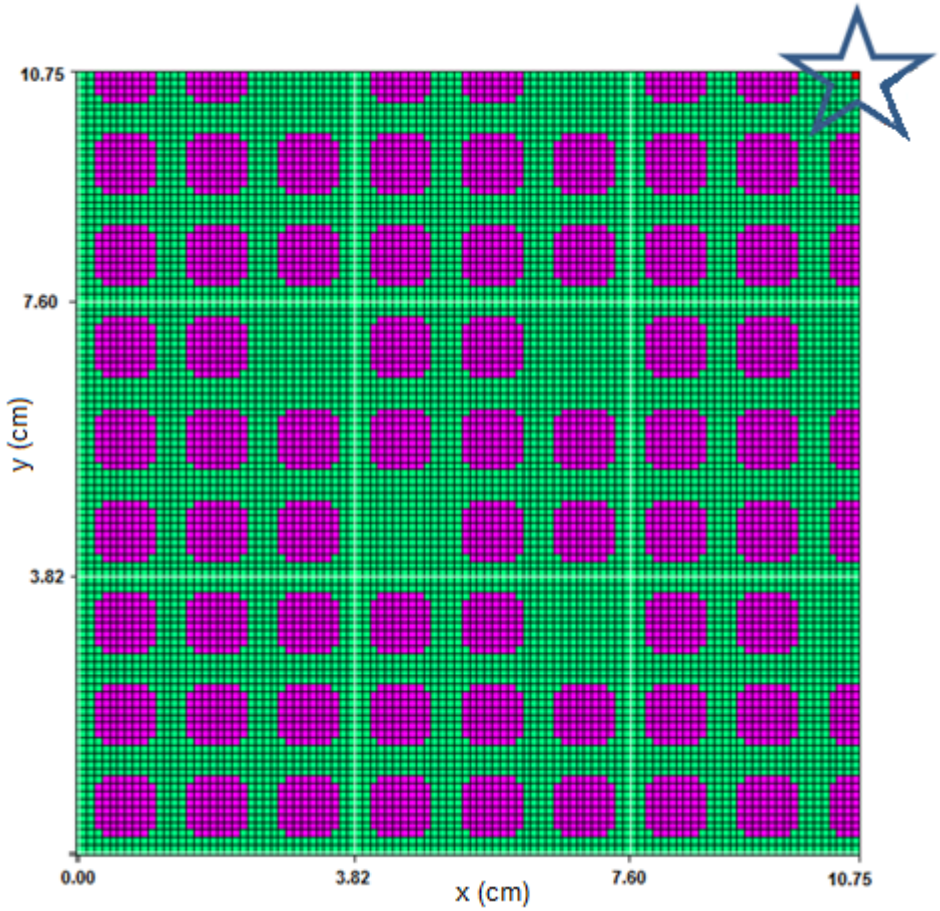

Figure 3-1. PWR quarter assembly view with SiC detector (top right mesh).

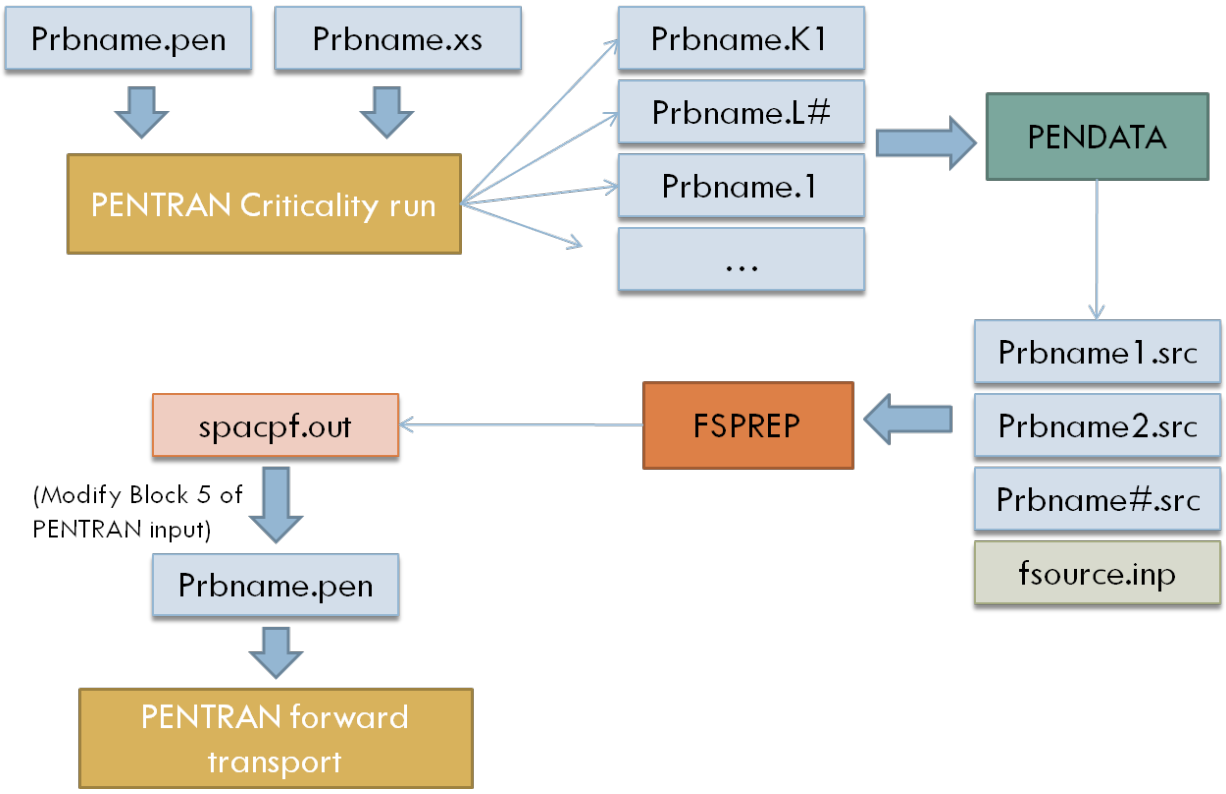

Figure 3-2. Flow path with FSPREP to generate fixed source.

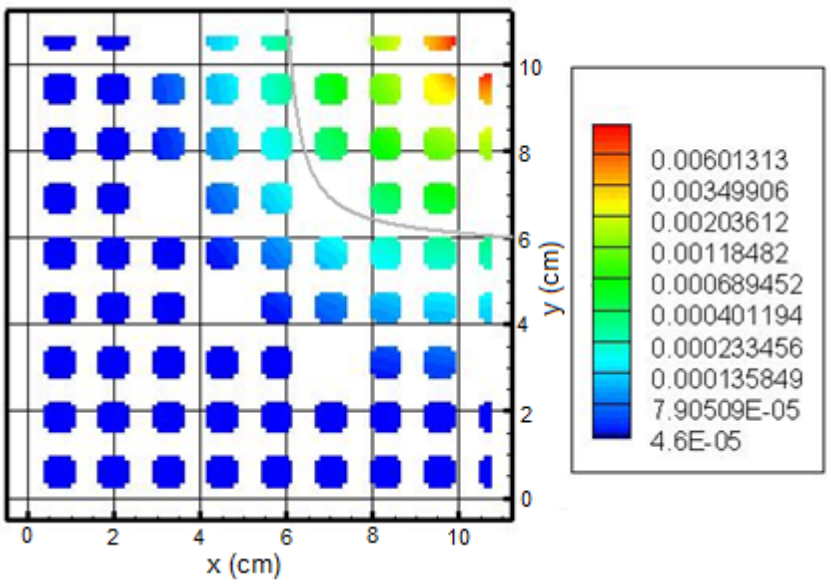

Figure 3-3. Normalized adjoint results for the thermal group (E<0.625 eV).

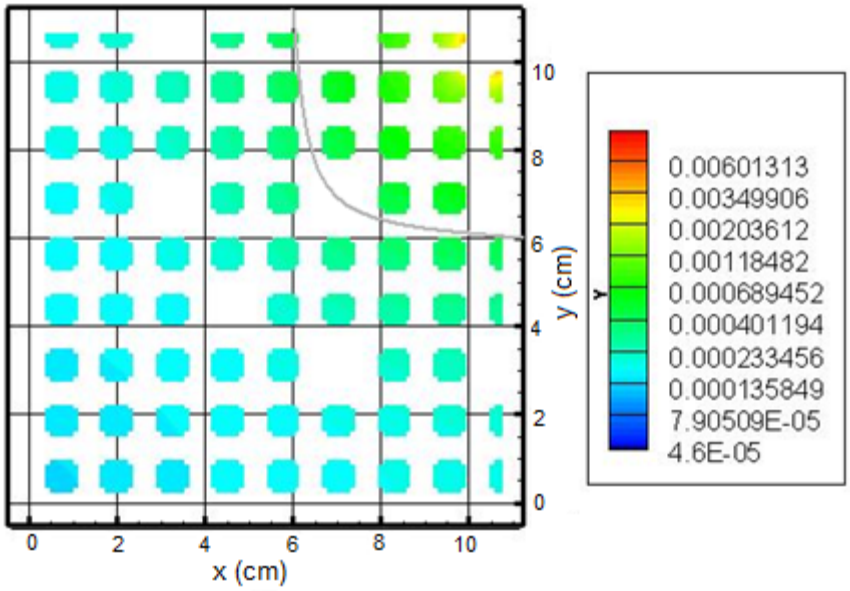

Figure 3-4. Normalized adjoint results for the epithermal group (0.625eV < E < 1.01 MeV).

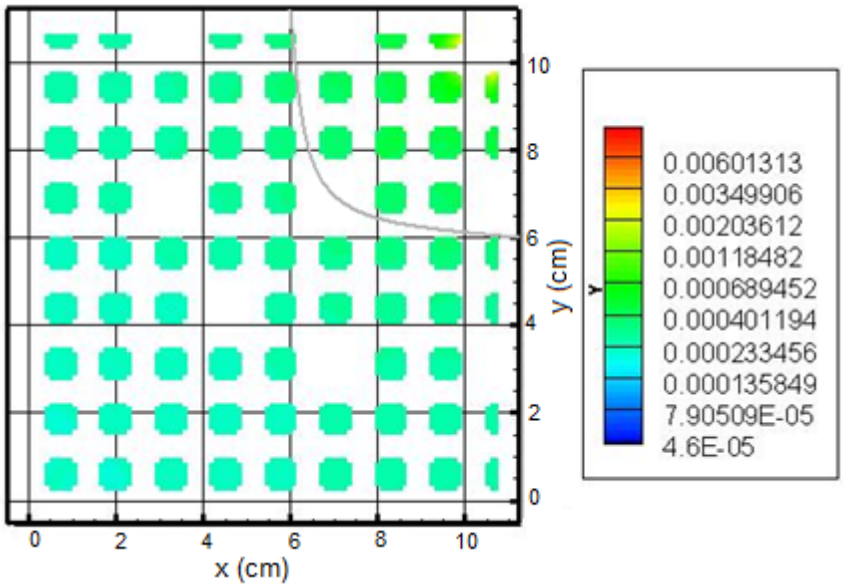

Figure 3-5. Normalized adjoint results for the fast group (E > 20 MeV).

CHAPTER 4
PENTRAN/PENBURN ANALYSIS OF A SINGLE BWR FUEL ROD

Efforts to accurately represent the fissile material quantities can quickly increase memory requirements for 3-D deterministic calculations. For a full core model deterministic analysis, parallel computing is a needed feature for even 2-D geometries. In order to accurately represent burnup distributions axially in a BWR, it imperative that we model in 3-D, particularly because of the changing void fraction along the axial dimension.

4.1 Steady State Two Phase Flow in a Heated Channel

To account for the two-phase flow that the water undergoes in a BWR, a solver was created that determines the axial void distribution for any BWR model given the thermal output of the reactor, operating pressure, inlet and outlet coolant temperature, fuel height and the exit quality.

To further simplify the equations any pressure drop was neglected and sinusoidal heat generation was considered (Kazimi and Todreas, 1990). The specific heat with constant pressure, saturation temperature, saturated liquid enthalpy and saturated vapor enthalpy are determined with the given input parameters from available data given the operating parameters. Equations 4-1 to 4-14 indicate the equations used in the solver to determine the axial void distribution. These equations were developed assuming a sinusoidal behavior for the initial power profile and neglected control rod effects due to insufficient rod positioning data. Figure 4-1 displays a coordinate system reference for the solver where z=0 represents the midline of the core.

$$h_{fg} = h_g - h_f \tag{4-1}$$

$$h_{in} = h_f - (C_p(T_f - T_{in})) \tag{4-2}$$

$$h_{out} = h_f + (X_{out} - h_{fg}) \tag{4-3}$$

$$X_{out} = X_{in} + \frac{q}{2mh_{fg}}\left[\sin\left(\frac{\pi z_{out}}{L}\right) + 1\right] \quad (4\text{-}4)$$

$$h_{out} = h_{in} + \frac{q}{2m}\left[sin\left(\frac{\pi z_{out}}{L}\right) + 1\right] \quad (4\text{-}5)$$

$$X_{in} = \frac{h_{in} - h_f}{h_{fg}} \quad (4\text{-}6)$$

$$q = \frac{2m(h_f - h_{in})}{sin\left(\frac{\pi Z_b}{L}\right)+1} \quad (4\text{-}7)$$

$$Z_b = \frac{L}{\pi}\sin^{-1}\left[-1 + 2\left(\frac{h_f - h_{in}}{h_{out} - h_{in}}\right)\right] \quad (4\text{-}8)$$

$$z_{out} = \frac{L}{2} \quad (4\text{-}9)$$

$$m = \frac{q}{h_{out} - h_{in}} \quad (4\text{-}10)$$

$$h_f - h_{in} = \frac{q}{2m}\left[\sin\left(\frac{\pi Z_b}{L}\right) + 1\right] \quad (4\text{-}11)$$

$$Z_b = \frac{L}{\pi}\sin^{-1}\left[-1 + \frac{2m}{q}\left(h_f - h_{in}\right)\right] \quad (4\text{-}12)$$

$$X_z = Xin + \frac{q}{2mh_{fg}}\left[\sin\left(\frac{\pi z}{L}\right) + 1\right] \quad (4\text{-}13)$$

$$\alpha_z = \frac{1}{1+\frac{\rho_v}{\rho_l}\left(\frac{1-X_z}{X_z}\right)} \quad (4\text{-}14)$$

Where q = Thermal output (kW)
P = System Pressure (Pa)
T_{in} = Inlet Temperature (°C)
T_{out} = Outlet Temperature (°C)
L = Fuel Height (m)
X_{out} = Exit quality of the core
C_p = Specific Heat Constant Pressure (kJ/kgK)
T_{sat} = Saturation Temperature (°C)
h_f = Saturated liquid enthalpy (kJ/kg)
h_g = Saturated vapor enthalpy (kJ/kg)
h_{fg} = Saturated enthalpy (kJ/kg)
h_{in} = Inlet enthalpy (kJ/kg)
h_{out} = Outlet enthalpy (kJ/kg)
X_{in} = Inlet quality of the core
m = mass flow rate (kg/s)
zout = Top of core (m)

z_b = Non-boiling length (m)
X_z = Quality of the core along axial direction z
z = Axial location (m)
α_z = Axial void fraction along axial direction z
ρ_v = Saturated vapor density
ρ_l = Saturated liquid density

4.2 Axial Distribution of Vapor Quality in a BWR Assembly

Using the thermal-hydraulics characteristics of a typical BWR/6 assembly of 3579 MWth, 7.17 MPa, an inlet coolant temperature of 277 C, an outlet coolant temperature of 286 C, fuel length of 3.7592 m, and an exit quality of 0.146, the axial void distribution was determined. Figure 4-2 displays the axial distribution of the void fraction determined from the solver. The figure expresses that the void fraction is zero (the coolant is 100% liquid) from the bottom of the core to around 1.1 meters where the coolant begins to transition to steam.

4.3 Single Pin Burnup Comparison with SFCOMPO

Utilizing the burnup history from the SFCOMPO data set, a preliminary effective 2-D single fuel pellet analysis was analyzed with PENBURN with a moderator density at 0.74153 g/cm^3 at an axial height of 44 cm, and the other with a moderator density at 0.33973 g/cm^3 and an axial height of 268 cm. A comparison between using initial cross sections versus burnup dependent cross sections was also investigated, and results for these are shown in Table 4-1 and Table 4-2, respectively. Although the burnup dependent cross sections decreased the percent differences of the PENBURN single pin burnup results relative to the SFCOMPO results at that pin location, with a significant decrease in the Pu-241 percent difference, there were still large differences noted between a single fuel pellet and the SFCOMPO results. It is evident that moving to a full 3-D model would be necessary to represent the flux at the multiple locations. When comparing a fuel pellet burnup with a water density of 0.74153 g/cm^3 at the 268 cm height the burnup results agreed within 30% of the SFCOMPO data as displayed in Table 4-3.

4.4 BWR Fuel Rod Axial Zone Optimization

Once the axial distribution of the vapor quality was determined the model was partitioned to contain a different water density in each region. After performing a transport calculation it was apparent from the flux shown in Figure 4-3 that consideration should be taken when choosing the number of varying water regions to use for the problem. The initial number of water densities used displayed step decreases at locations where the water density was lower and would not represent what occurs in a typical BWR fuel assembly. Multiple transport calculations were performed to determine the minimum number of water densities required for an accurate initial model for the BWR fuel rod. Results indicated that a minimum of seven different water regions from 0.7 g/cm^3 to 0.2 g/cm^3 was necessary with no more than a 0.1 g/cm^3 decrease from region to region. The results from this partitioning are shown in Figure 4-4.

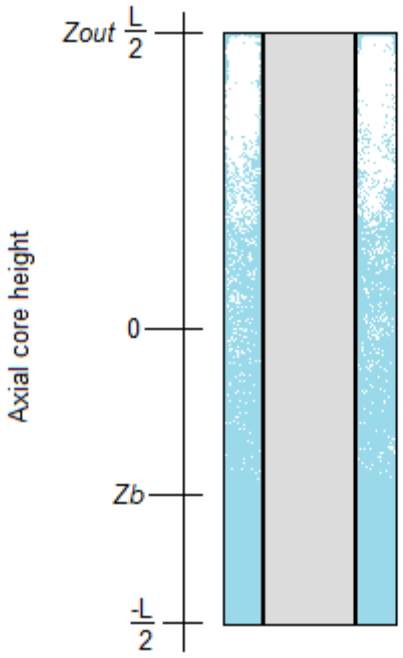

Figure 4-1. Coordinate system reference for axial void solver where z=0 represents midpoint of core.

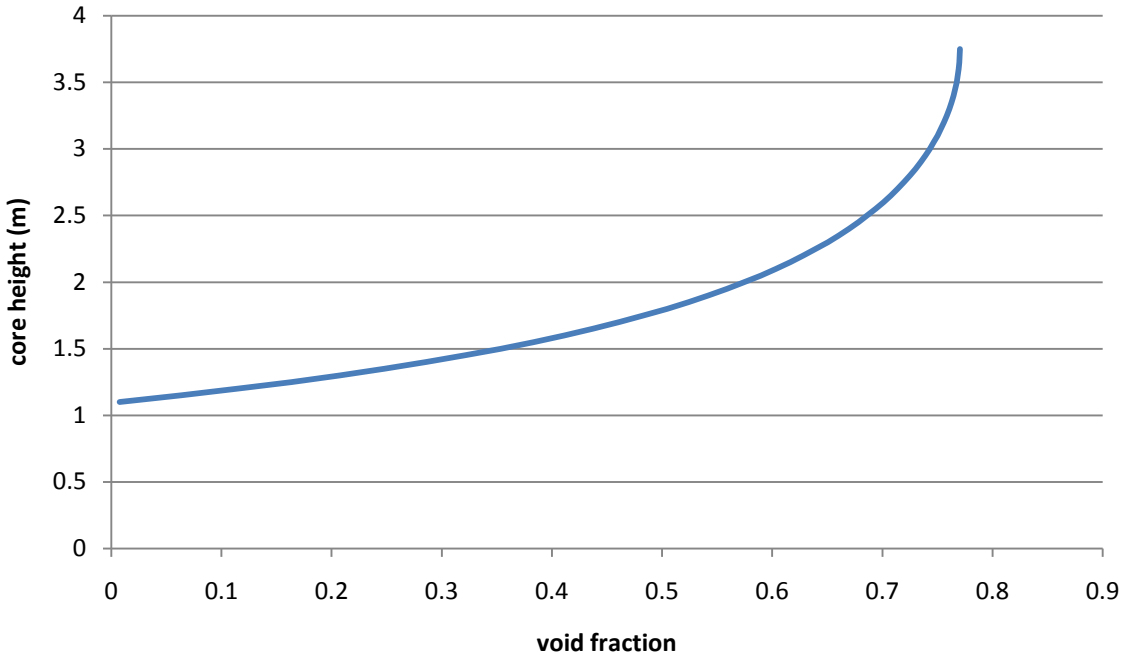

Figure 4-2. Void fraction distribution in a typical BWR/6 assembly.

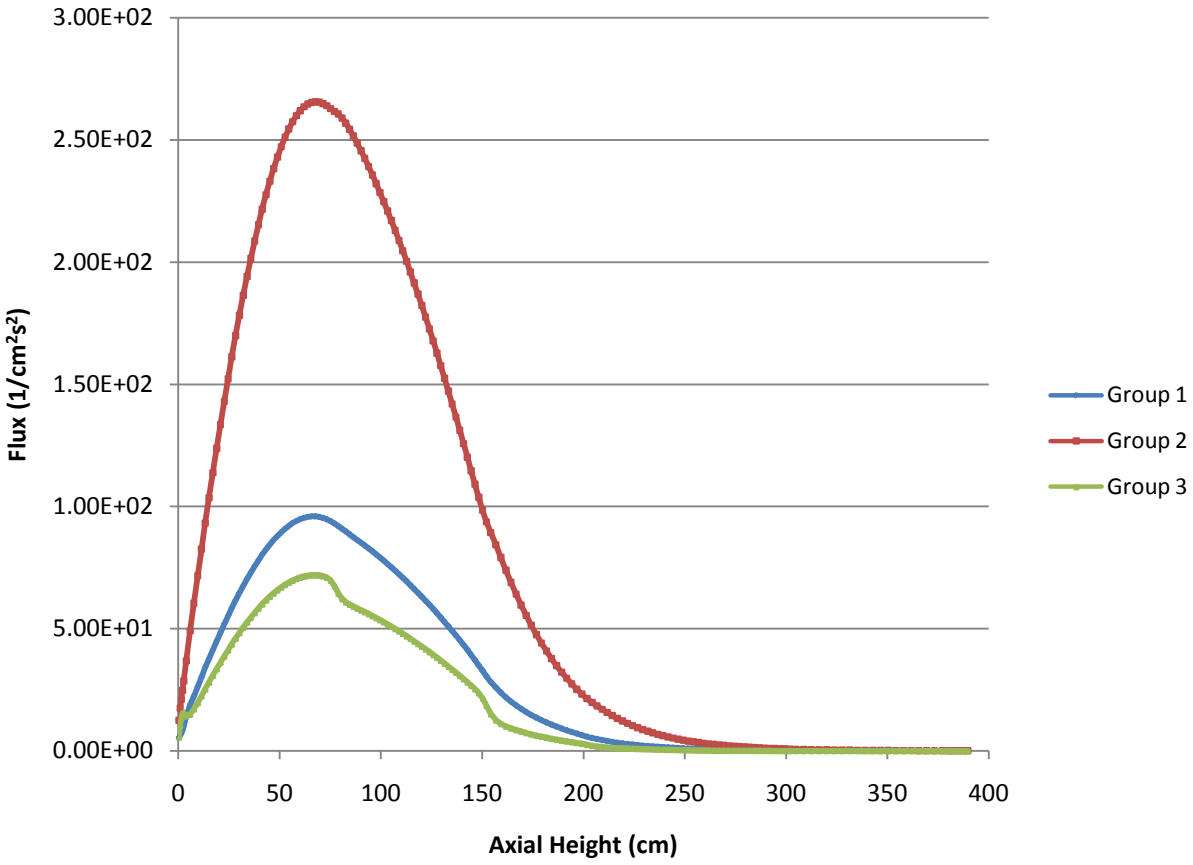

Figure 4-3. Initial flux at centerline of BWR/6 pin for case with six different moderator densities around fuel assembly.

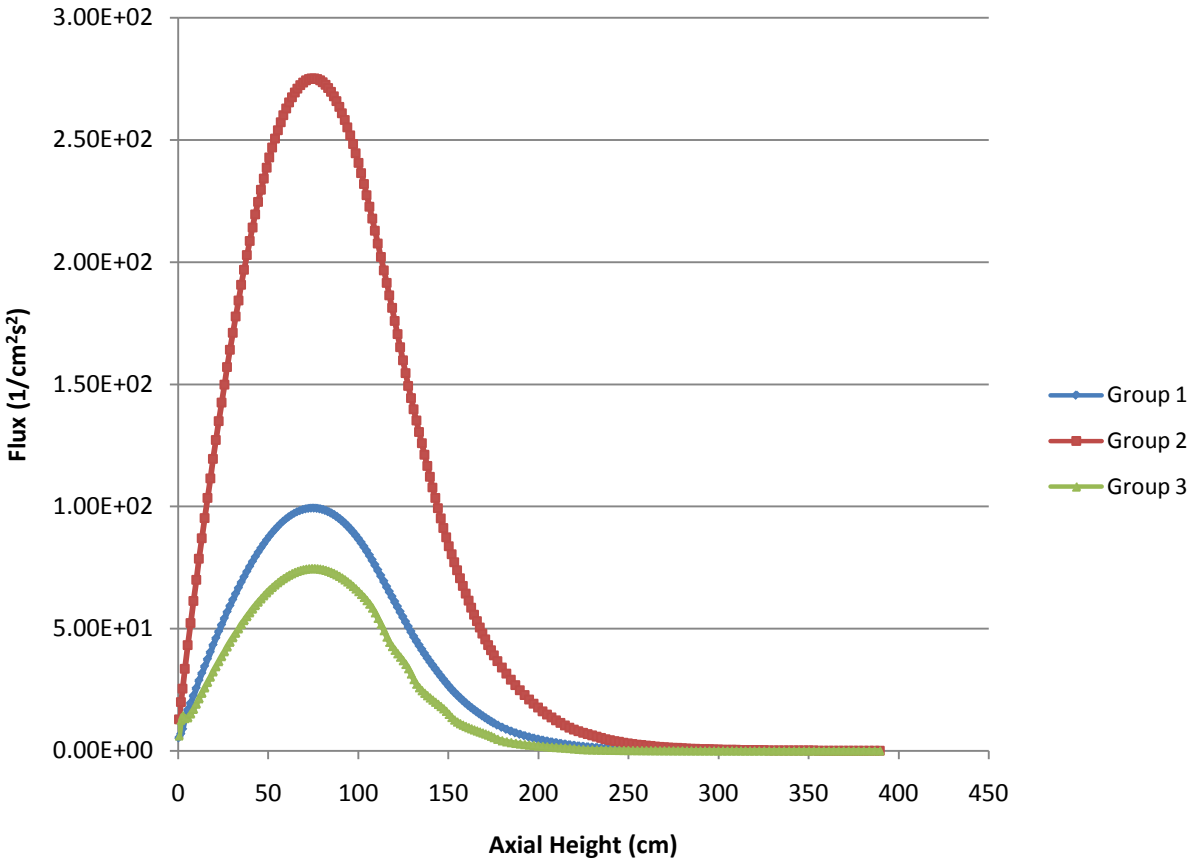

Figure 4-4. Optimum axial zone distribution in a typical BWR/6 assembly.

Table 4-1. A1 fuel element at 44 cm 0.74153 g/cc percent differences between SFCOMPO values and PENBURN burnup results (22.6 GWD/MTU)

Data Type	SFCOMPO Values	Percent Difference	
		initial-xs	burnup-xs
Pu-239/Total Pu(RateOfWeight)	5.56E-01	43.56%	40.73%
Pu-239/U-238	3.89E-03	275.73%	258.53%
Pu-240/Pu-239	4.88E-01	-87.86%	-78.32%
Pu-240/Total Pu(RateOfWeight)	2.69E-01	-82.42	-69.23%
Pu-241/Pu-239	1.87E-01	-7.83%	-19.57%
Pu-241/Total Pu(RateOfWeight)	1.17E-01	17.58%	0.58%
Pu-242/Pu-239	9.01E-02	-76.41%	-75.80%
Pu-242/Total Pu(RateOfWeight)	4.85E-02	-65.02%	-64.82%
Total Pu/Total U	6.93E-03	160.10%	153.17%
U-235/Total U(RateOfWeight)	6.61E-03	91.63%	88.73%
U-235/U-238	6.76E-03	90.36%	87.48%
U-236/Total U(RateOfWeight)	3.41E-03	-12.29%	-6.93%
U-236/U-238	3.46E-03	-12.18%	-6.81%
U-238/Total U(RateOfWeight)	9.90E-01	-0.57%	-0.57%

Table 4-2. B3 fuel pellet at 268 cm 0.33973 g/cc percent differences between SFCOMPO values and PENBURN burnup results (22.6 GWD/MTU)

Data Type	SFCOMPO Values	Laboratory	Percent Difference Initial-xs	Percent Difference burnup-xs
Pu-239/Total Pu(RateOfWeight)	0.638	Karlsruhe	25.11%	22.65%
Pu-239/Total Pu(RateOfWeight)	0.641	Ispra	24.52%	22.07%
Pu-239/U-238	0.0057	Karlsruhe	158.69%	146.85%
Pu-239/U-238	0.0055	Ispra	163.83%	151.75%
Pu-240/Pu-239	0.345	Karlsruhe	-82.83%	-69.34%
Pu-240/Pu-239	0.345	Ispra	-82.83%	-69.34%
Pu-240/Total Pu(RateOfWeight)	0.221	Karlsruhe	-78.61%	-62.55%
Pu-240/Total Pu(RateOfWeight)	0.219	Ispra	-78.41%	-62.21%
Pu-241/Pu-239	0.143	Karlsruhe	20.53%	5.17%
Pu-241/Pu-239	0.147	Ispra	17.25%	2.31%
Pu-241/Total Pu(RateOfWeight)	0.104	Karlsruhe	32.28%	13.16%
Pu-241/Total Pu(RateOfWeight)	0.104	Ispra	32.28%	13.16%
Pu-242/Pu-239	0.0414	Karlsruhe	-48.67%	-47.33%
Pu-242/Pu-239	0.0418	Ispra	-49.16%	-47.83%
Pu-242/Total Pu(RateOfWeight)	0.0264	Karlsruhe	-35.75%	-35.37%
Pu-242/Total Pu(RateOfWeight)	0.0261	Ispra	-35.01%	-34.63%
Total Pu/Total U	0.0088	Karlsruhe	106.00%	100.51%
Total Pu/Total U	0.0085	Ispra	111.81%	106.17%
U-235/Total U(RateOfWeight)	0.0104	Karlsruhe	21.80%	19.95%
U-235/Total U(RateOfWeight)	0.0102	Ispra	24.19%	22.31%
U-235/U-238	0.0105	Karlsruhe	22.56%	20.70%
U-235/U-238	0.0103	Ispra	24.94%	23.04%
U-236/Total U(RateOfWeight)	0.0031	Karlsruhe	-2.89%	3.05%
U-236/Total U(RateOfWeight)	0.0031	Ispra	-2.26%	3.72%
U-236/U-238	0.0031	Karlsruhe	-2.61%	3.34%
U-236/U-238	0.0031	Ispra	-2.30%	3.67%
U-238/Total U(RateOfWeight)	0.987	Karlsruhe	-0.27%	-0.27%
U-238/Total U(RateOfWeight)	0.987	Ispra	-0.27%	-0.27%

Table 4-3. B3 fuel pellet at 268 cm 0.74153 g/cc percent differences between SFCOMPO values and PENBURN burnup results (22.6 GWD/MTU)

Data Type	SFCOMPO Values	Measurement Laboratory	Percent Difference	
			Initial-xs	Burnup-xs
Pu-239/Total Pu(RateOfWeight)	6.38E-01	Karlsruhe	4.84%	6.22%
Pu-239/Total Pu(RateOfWeight)	6.41E-01	Ispra	4.35%	5.72%
Pu-239/U-238	5.65E-03	Karlsruhe	10.16%	25.76%
Pu-239/U-238	5.54E-03	Ispra	12.34%	28.26%
Pu-240/Pu-239	3.45E-01	Karlsruhe	-46.52%	-23.70%
Pu-240/Pu-239	3.45E-01	Ispra	-46.52%	-23.70%
Pu-240/Total Pu(RateOfWeight)	2.21E-01	Karlsruhe	-44.16%	-19.28%
Pu-240/Total Pu(RateOfWeight)	2.19E-01	Ispra	-43.65%	-18.54%
Pu-241/Pu-239	1.43E-01	Karlsruhe	77.16%	20.94%
Pu-241/Pu-239	1.47E-01	Ispra	72.34%	17.64%
Pu-241/Total Pu(RateOfWeight)	1.04E-01	Karlsruhe	62.94%	12.69%
Pu-241/Total Pu(RateOfWeight)	1.04E-01	Ispra	62.94%	12.69%
Pu-242/Pu-239	4.14E-02	Karlsruhe	38.15%	-4.82%
Pu-242/Pu-239	4.18E-02	Ispra	36.83%	-5.73%
Pu-242/Total Pu(RateOfWeight)	2.64E-02	Karlsruhe	44.91%	1.15%
Pu-242/Total Pu(RateOfWeight)	2.61E-02	Ispra	46.57%	2.32%
Total Pu/Total U	8.75E-03	Karlsruhe	4.94%	18.25%
Total Pu/Total U	8.51E-03	Ispra	7.90%	21.58%
U-235/Total U(RateOfWeight)	1.04E-02	Karlsruhe	-0.91%	-2.35%
U-235/Total U(RateOfWeight)	1.02E-02	Ispra	1.03%	-0.43%
U-235/U-238	1.05E-02	Karlsruhe	-0.54%	-1.99%
U-235/U-238	1.03E-02	Ispra	1.39%	-0.08%
U-236/Total U(RateOfWeight)	3.08E-03	Karlsruhe	-5.74%	-2.66%
U-236/Total U(RateOfWeight)	3.06E-03	Ispra	-5.13%	-2.02%
U-236/U-238	3.12E-03	Karlsruhe	-5.71%	-2.63%
U-236/U-238	3.11E-03	Ispra	-5.40%	-2.31%
U-238/Total U(RateOfWeight)	9.87E-01	Karlsruhe	-0.02%	-0.02%
U-238/Total U(RateOfWeight)	9.87E-01	Ispra	-0.02%	-0.02%

CHAPTER 5
GUNDREMMINGEN ASSEMBLY ANALYSIS

After developing methods for determining the multigroup cross sections for a BWR and achieving the optimum axial zone partitioning, the Gundremmingen BWR was chosen as the candidate design for performing the burnup calculations to compare to SFCOMPO. Again, the major purpose here was to characterize the general effects of fuel burnup on the BWR case. The impact of slight changes to moderator density on spent fuel isotopics was investigated and improvements to the model discussed.

5.1 BWR Assembly Specifications

Based on the operating parameters in Table 5-1 the inlet water density was calculated as 0.74153 g/cm^3 and the outlet water density as 0.289 g/cm^3 using the solver discussed in Chapter 4. The axial void fraction, quality and density distributions are displayed in Figures 5-1, 5-2, and 5-3 respectively. The PENTRAN model was partitioned with 7 different water densities as discussed previously and the different regions can be seen in Figure 5-4. Assembly B23 was chosen to compare PENBURN burnup results with the results from the SFCOMPO database. This assembly primarily remained in the lower right hand side of the core for all 4 cycles as presented in Figure 5-5. The Gundremmingen BWR assembly consists of a 6x6 array of fuel rods with enrichments of either 1.87 or 2.53 percent as demonstrated from the Tecplot generated image shown in Figure 5-6. Due to a lack of information, the use of control rods was not taken into account in this analysis.

5.1.1 Fuel Pin Homogenization

Analysis was performed to determine the optimum meshing scheme for homogenizing the fuel, gap and clad into one material. This was performed in order to save on memory requirements when moving from a single full length fuel rod to the entire BWR assembly. Table

5-2 contains the homogenized fuel composition data. The resulting meshing went from 19x19 to 11x11 and still maintained a reasonable mass balance in addition to agreeable eigenvalue results between PENTRAN and SCALE as shown in Table 5-3. The multigroup cross sections were generated for each of the water densities from the same procedure discussed in Chapter 2 and the SCALE 5.1 keff results for each region are in Table 5-4.

5.1.2 PENTRAN Geometry

The 6x6 Gundremmingen BWR assembly was partitioned into 10 axial z-coarse meshes with a top and bottom water region. The middle 8 regions contained the fuel pins and the material numbers were assigned based on water density. Therefore fuel pins 1 through 36 were surrounded by the denser water, and fuel pins 217 to 252 were the pins surrounded by the water region with the largest void fraction. The 3-D relative flux profile by energy group at 0.00 GWD/MTU is illustrated in Figure 5-7 and exhibits the skewed flux as a result of the initial void fraction distribution. Figure 5-8 contains the 3-D relative flux profiles at around a meter above the bottom of the core with the water material locations blanked out, and displays how the epithermal group experienced the highest flux values. Recalling the fuel pins on the left corner of the image are initially of lower enrichment, it is evident the 3-D flux profile contains information that would be lost in a 2-D representation of the assembly.

5.2 MCNP Criticality Calculation

In order to compare the PENTRAN criticality run with the MCNP criticality calculation the XSMCNP code was utilized to convert the macroscopic cross sections from the PENTRAN format into the MCNP multigroup format. The code asks the user for the PENTRAN cross section file name, the Pn order of the cross section file, and the Pn order desired in the MCNP input deck. The only required input file is the PENTRAN macroscopic cross section file.

Optional input files include:

1. grp_erg.bnd : indicates energy group structure by specifying upper energy bound in each group (MeV) NOTE: group 1 is entered first
2. grp_mat.chi: contains the normalized fission spectrum data for each material and energy group
3. grp_mat.nu: includes the ν value for each material by energy group

Output files:

A. mgxs: MCNP multigroup cross section data file
B. xsdir: MCNP cross section isotope index file
C. mcnp.inp: A sample MCNP input file with generated material cards when using multigroup cross sections.

The ALPO module settings used previously were modified in order to extract ν data from the SCALE output files. The new ANISN format library output file contains the values for χ, σ_f, σ_a, $\nu\sigma_f$ and σ_t for each energy group. A sample input file for the ALPO input required to generate the additional information is in Appendix D. The ν values calculated from the extracted data can be found in Table 5-5. The fission spectrum was determined by using GMIX for all seven fuel regions. Appendix E contains a sample MCNP input deck containing the BWR assembly geometry. Using the resulting multigroup cross section file along with the MCNP input resulted in a k-eff value of 1.13323 a percent difference of 3.4% with the PENTRAN k-eff value. A total of 50,000 particles per cycle were used with 200 skipped cycles and a total of 1000 cycles. Different runs were performed as shown in Table 5-6 yet not all of the flux tally bins passed the ten statistical tests and some calculations reported large relative errors. This difference can be attributed to the fact that PENTRAN uses a Cartesian geometry to represent the problem setup and as a result the fissile mass in both models are different. In addition to this Monte Carlo experiences difficulty converging since the source is not known initially. There may have been a false source convergence which resulted in underestimating the k-eff value (Haghighat and Wagner 2003). Other factors contributing in differences include the method of

multigroup cross section generation when using a homogenized (fuel+gap+clad) fuel material surrounded by water. Comparing an MCNP model using the continuous energy cross section library with an MCNP model using the multigroup cross sections is useful to verify the collapsed library group structure.

5.3 BWR Assembly Burnup Results

The burnup steps chosen in Table 5-7 were modeled after the data provided form SFCOMPO. The fuel assembly remained in the reactor for 4 cycles with cooling times in between for a total of 22.3 GWD/MTU. Table 5-8 contains the k-eff result at the beginning of each burnup step. It is interesting to note that the k-eff value increases slightly and then starts decreasing again during two instances in the burnup steps; once during the second burnup step and another time during burnup step 21. This is most likely due to the shifting power profile that is a result of the changing void fraction in a BWR assembly. Initially the flux is extremely skewed with the peak flux towards the bottom of the assembly and as a result the fuel at the bottom experiences more burnup. As this continues the peak power begins to shift upwards towards the center of the assembly. This shifting power is seen assuming there were no control rods inserted next to the fuel assembly during the cycle length since there is no data available regarding control rod use for this reactor.

The output from PENBURN was compared to SFCOMPO post irradiation results for the fuel material numbers of interest as indicated in Table 5-9. Differences between the two are shown in the subsequent tables. One thing to note however was that the burnup reported for the fuel element sometimes differed from the average burnup calculated from the amount of time the fuel assembly was in the reactor. For instance, for fuel element A1 the lab reported a burnup of 25.7 GWD/MTU, a value significantly larger than the 22.6 GWD/MTU used in the burnup simulation. The U-238 results consistently agreed with the SFCOMPO data, while there were

significant differences overall with the other data values. These differences can be attributed to insufficient data regarding control rod movements in the BWR in addition to not using burnup dependent cross sections for the burnup steps in this comparison. Since the control rod data is unavailable, one step to take to more accurately represent physics of the problem was to generate the burnup dependent cross sections.

5.4 Burnup Dependent Cross Section Generation

The DEV-XS procedure outlined previously was utilized to generate the burnup dependent cross sections. This time however the t-depl control sequence was used to extract burnup dependent cross sections at specific burnup points. The minimum number of burnup points to consider had been determined from a previous study (Plower, 2008). A library was generated at 0, 0.0459, 17.85, 26.35 GWD/MTU burnup points and at fuel temperatures of 900 and 1000 K. Modifications to the previous SCALE input were necessary in order to save the collapsed cross sections at each burnup step. Initially the user should include savlib in the parm input and indicate parm=(savlib,addnux=3). The user should not include a space between the savlib and addnux keywords otherwise SCALE 5.1 fails to recognize the addnux keyword and no additional nuclides will be added to the cross section database. A burnup data block was set to generate the collapsed cross sections at the desired burnup points. SCALE uses a predictor corrector approach when running the burnup sequence and therefore outputs data at the midpoint of each burnup length. SCALE also does not allow the user to exceed 8.647 GWD/MTU between burnup steps. For this reason, the number of days for each burnup step was chosen as 40, 300, 300, 272, 200 and 68 days with 23 W/g. If the user exceeds the 8.647 GWD/MTU between burnup steps SCALE automatically increases the number of burnup steps and the user may confuse which collapsed cross section file corresponds to a specific burnup point. It is important to note that the collapsed cross sections saved at each burnup point are obtained when using

modified versions of TRITON and PMC obtained from ORNL. A sample SCALE 5.1 input file to generate burnup dependent cross sections is in Appendix F, while Appendix G contains the APLO input required to format the multiple cross section files at the different burnup points.

5.5 Accounting for Power Shift

The initial relative flux as a function of energy group at the centerline of the fuel rod located in position A1 is displayed in Figure 5-9. As burnup progresses however there is a power shift as the peak progresses upward along the assembly due to the burnout of U-235. The power shift continues to occur until the peak flux is seen at outer edges with a dip in the middle of the fuel rod after 5.83 GWD/MTU. Then at 7.73 GWD/MTU, the peak flux in group 2 is no longer at a core height of 100 cm but has shifted to a peak flux location at the core height of 200 cm. Figures 5-10 through 5-14 contain the relative flux profile by energy group at the centerline of fuel pin A1 at different burnup points. Due to this power shift, the water density at each axial zone should be repositioned beginning after 3.74 GWD/MTU of burnup. This can be accomplished by implementing a coupled thermal hydraulic and transport step during the PENTRAN/PENBURN burnup sequence. A new void fraction distribution solver should be created which takes into account the new power profile as opposed to a sinusoidal shape. Therefore one could obtain a new axial enthalpy equation based on the power shape, the enthalpy as a function of axial height takes the form of Equation 5-1. And the quality at any axial position would be determined from Equation 5-2.

$$h(z) = h_{in} + \frac{q}{2m}[f(z)] \tag{5-1}$$

$$x(z) = x_{in} + \frac{q}{2mh_{fg}}[f(z)] \tag{5-2}$$

Where, $h(z)$= enthalpy as a function of axial height z(kJ/kg)
z= axial height location (m)
h_{in}= enthalpy at the inlet (kJ/kg)
q= thermal output (kW)

m= mass flow rate (kg/s)
f(z)=normalized flux from transport calculation as a function of axial height z
x(z)= quality as a function of axial height z
x_{in}= quality at inlet
h_{fg}= saturated enthalpy (kJ/kg)

After a transport calculation is completed, the resulting power profile can be utilized with these equations to determine the void distribution once the power profile changes. Since the flux profile changes as a function of burnup, the most effective way to perform this new calculation is by implementing a coupled thermal hydraulic and transport solver method at every burn step. An efficient way to perform this calculation is by creating a driver to apply this new step to the calculations.

Table 5-1. Gundremmingen BWR assembly specifications

Power	250 MWe
Water density at bottom (g/cm^3)	0.74153
Average density of fuel	10.50
Fuel enrichment	1.87/2.53
Homogenized fuel pellet diameter (cm)	1.4280
Fuel rod pitch (cm)	1.7800
Clad material	Zr-2
Length of fuel rods (cm)	3.30E+02
Rod array	6x6
Number of rods	36
Side of square fuel section (cm)	11.3520
Assembly fuel channel thickness (cm)	0.3350
Number of assemblies	368
Inlet temperature (C)	266
Outlet temperature (C)	286

Table 5-2. Fuel composition of homogenized fuel

	Enrichment	
	2.53	1.87
Nuclide	Wt%	Wt%
O^{16}	9.8977	9.8969
U^{234}	0.0169	0.0169
U^{235}	1.8622	1.3764
U^{236}	0.0088	0.0088
U^{238}	71.7204	72.2070
He^4	0.0256	0.0256
Nat. zirc	16.4681	16.4681
Total	100	100

Table 5-3. Homogenized fuel PENTRAN and SCALE comparison

Eigenvalue (PENTRAN)	% difference from SCALE (1.23210)	% excess fissile material
1.230234	-0.15%	-0.27%

Table 5-4. SCALE 5.1 keff values by water density region

density (g/cm^3)	keff
0.74153	1.23210
0.72039	1.22614
0.64761	1.20311
0.54668	1.16336
0.44533	1.11133
0.33973	1.03885
0.28956	0.99551

Table 5-5. Nubar data by fuel region

	Group		
fuel zone	fast	epithermal	thermal
1	2.78402	2.43631	2.43663
2	2.78358	2.43620	2.43666
3	2.78216	2.43625	2.43656
4	2.78016	2.43629	2.43682
5	2.77762	2.43636	2.43674
6	2.77451	2.43650	2.43667
7	2.77263	2.43662	2.43669

Table 5-6. MCNP particle histories

# particles/hist	# ksrc pts.	Cycles Skipped	Total Cycles	keff	Error	Stat. Test Not Passed	Large Rel. Error
10000	1764	100	300	-	-	4	3
100000	1764	200	500	-	-	7	3
5000	2340	200	500	-	-	6	4
100000	2484	200	600	1.13319	0.00017	2	0
50000	2484	200	1000	1.13274	0.00017	1	0
50000	3024	200	1000	1.13292	0.00016	3	1
50000	7452	200	1000	1.13323	0.00016	1	0

Table 5-7. Gundremmingen B23 assembly operation history

Cycle of Operation	Periods	Days	Core Burnup (MWD/MTU)
Second	8/25/1969 5/30/1970	279	5839
Shutdown	5/31/1970 7/24/1970	56	-
Third	7/25/1970 6/12/1970	323	6131
Shutdown	6/13/1971 7/15/1971	33	-
Fourth	7/16/1971 4/30/1972	290	5483
Shutdown	5/1/1972 6/30/1972	61	-
Fifth	7/1/1972 5/5/1973	309	5174

Table 5-8. Burnup steps with keff results

Step	W/g	days	Burnup (GWD/MTHM)	keff	error
1	-20.928	1	0.020928	1.17451	-8.89E-05
2	-20.928	1	0.041857	1.17636	7.98E-05
3	-20.928	1	0.062785	1.17578	7.66E-05
4	-20.928	1	0.083713	1.17507	-7.96E-05
5	-20.928	3	0.146498	1.17448	-7.30E-05
6	-20.928	12	0.418566	1.17313	8.58E-05
7	-20.928	40	1.255698	1.16756	8.46E-05
8	-20.928	40	2.09283	1.14725	9.55E-05
9	-20.928	80	3.746166	1.12539	7.85E-05
10	-20.928	100	5.838996	1.01876	8.39E-05
11	0	56	5.838996		
12	-18.981	100	7.737136	1.01876	8.39E-05
13	-18.981	100	9.635276	0.9742	-7.79E-05
14	-18.981	123	11.969988	0.95017	7.15E-05
15	0	33	11.969988		
16	-18.907	90	13.671609	0.93533	-2.02E-05
17	-18.907	100	15.562299	0.92192	-5.73E-05
18	-18.907	100	17.452989	0.91524	7.95E-05
19	0	61	17.452989		
20	-16.744	100	19.127419	0.90964	6.73E-05
21	-16.744	100	20.801849	0.91091	6.27E-05
22	-16.744	109	22.626978	0.91094	-1.72E-05

Table 5-9. PENTRAN material numbers corresponding to SFCOMPO analyzed fuel

Location (cm)	density (g/cm^3)	A1	B3	B4	C5	E3	E5
44	0.74153	31	20	14	9	23	11
268	0.33973	211	200	194	189	203	191

Table 5-10. A1 fuel element at 44 cm percent difference between SFCOMPO values and PENBURN burnup results (SFCOMPO reports 25.7 GWD/MTU)

Data Type	SFCOMPO Values	Percent Difference	
		initial-xs	burnup-xs
Cs-137/U-238	2.12E-03	-87.72%	-81.83%
Nd-148/U-238	4.88E-04	-84.13%	-77.97%
Pu-239/Total Pu(RateOfWeight)	5.56E-01	10.30%	-0.63%
Pu-239/U-238	3.89E-03	16.98%	-1.52%
Pu-240/Pu-239	4.88E-01	-67.97%	-39.67%
Pu-240/Total Pu(RateOfWeight)	2.69E-01	-41.89%	9.44%
Pu-241/Pu-239	1.87E-01	52.08%	8.48%
Pu-241/Total Pu(RateOfWeight)	1.17E-01	49.07%	-4.20%
Pu-242/Pu-239	9.01E-02	1.31%	-17.60%
Pu-242/Total Pu(RateOfWeight)	4.85E-02	15.43%	-15.42%
Total Pu/Total U	6.93E-03	6.35%	-0.63%
U-235/Total U(RateOfWeight)	6.61E-03	-52.24%	-52.95%
U-235/U-238	6.76E-03	-52.98%	-53.68%
U-236/Total U(RateOfWeight)	3.41E-03	5.61%	8.33%
U-236/U-238	3.46E-03	4.79%	7.49%
U-238/Total U(RateOfWeight)	9.90E-01	0.33%	0.32%

Table 5-11. A1 fuel element at 268 cm percent differences between SFCOMPO values and PENBURN burnup results(SFCOMPO reports 27.4 GWD/MTU)

Data Type	SFCOMPO Values	Percent Difference			
		initial-xs	burnup-xs	burnup-xs	burnup-xs
		.33 g/cc	.33 g/cc	.445 g/cc	.546 g/cc
Cs-137/U-238	1.67E-03	-85.72%	-87.81%	-76.99%	-81.60%
Nd-148/U-238	5.22E-04	-86.43%	-88.43%	-79.88%	-83.75%
Pu-239/Total Pu(RateOfWeight)	5.55E-01	46.78%	50.73%	38.54%	38.74%
Pu-239/U-238	4.99E-03	29.60%	36.38%	25.97%	13.94%
Pu-240/Pu-239	4.41E-01	-81.87%	-74.65%	-60.86%	-61.11%
Pu-240/Total Pu(RateOfWeight)	2.50E-01	-73.95%	-62.60%	-46.92%	-47.17%
Pu-241/Pu-239	1.97E-01	-32.52%	-61.33%	-43.71%	-44.13%
Pu-241/Total Pu(RateOfWeight)	1.31E-01	-17.34%	-51.35%	-34.92%	-35.31%
Pu-242/Pu-239	8.64E-02	-83.04%	-91.37%	-80.24%	-80.19%
Pu-242/Total Pu(RateOfWeight)	5.13E-02	-76.73%	-87.84%	-74.41%	-74.31%
Total Pu/Total U	8.95E-03	-12.73%	-10.60%	-9.72%	-18.45%
U-235/Total U(RateOfWeight)	7.09E-03	89.36%	94.28%	14.47%	14.48%
U-235/U-238	7.27E-03	87.69%	92.65%	12.95%	12.95%
U-236/Total U(RateOfWeight)	3.42E-03	-22.32%	-20.37%	1.91%	1.91%
U-236/U-238	3.49E-03	-22.63%	-20.66%	1.04%	1.04%
U-238/Total U(RateOfWeight)	9.89E-01	-0.51%	-0.56%	-0.06%	-0.06%

Table 5-12. B3 fuel element at 268 cm percent differences between SFCOMPO values and PENBURN burnup results (SFCOMPO reports 21.2 GWD/MTU)

Data Type	Measurement Laboratory	Percent Difference		
		initial-xs	burnup-xs	burnup-xs
		.339 g/cc	.339 g/cc	.445 g/cc
Cs-137/U-238	Karlsruhe	-84.61%	-77.17%	-75.20%
Cs-137/U-238	Ispra	-84.31%	-76.72%	-74.71%
Nd-148/U-238	Karlsruhe	-82.41%	-75.87%	-73.91%
Pu-239/Total Pu(RateOfWeight)	Karlsruhe	27.70%	31.25%	20.41%
Pu-239/Total Pu(RateOfWeight)	Ispra	27.10%	30.64%	19.85%
Pu-239/U-238	Karlsruhe	14.43%	19.91%	11.07%
Pu-239/U-238	Ispra	16.71%	22.29%	13.28%
Pu-240/Pu-239	Karlsruhe	-76.82%	-67.74%	-49.77%
Pu-240/Pu-239	Ispra	-76.82%	-67.74%	-49.77%
Pu-240/Total Pu(RateOfWeight)	Karlsruhe	-70.52%	-57.83%	-39.76%
Pu-240/Total Pu(RateOfWeight)	Ispra	-70.25%	-57.44%	-39.21%
Pu-241/Pu-239	Karlsruhe	-7.12%	-47.20%	-22.24%
Pu-241/Pu-239	Ispra	-9.65%	-48.63%	-24.36%
Pu-241/Total Pu(RateOfWeight)	Karlsruhe	461.53%	273.93%	254.42%
Pu-241/Total Pu(RateOfWeight)	Ispra	461.53%	273.93%	254.42%
Pu-242/Pu-239	Karlsruhe	-64.66%	-82.22%	-58.48%
Pu-242/Pu-239	Ispra	-64.99%	-82.39%	-58.87%
Pu-242/Total Pu(RateOfWeight)	Karlsruhe	143.70%	43.61%	115.85%
Pu-242/Total Pu(RateOfWeight)	Ispra	-54.32%	-76.38%	-49.40%
Total Pu/Total U	Karlsruhe	-10.76%	-9.08%	-7.72%
Total Pu/Total U	Ispra	-8.25%	-6.52%	-5.12%
U-235/Total U(RateOfWeight)	Karlsruhe	29.20%	34.17%	-22.12%
U-235/Total U(RateOfWeight)	Ispra	31.73%	36.80%	-20.59%
U-235/U-238	Karlsruhe	30.06%	35.15%	-21.95%
U-235/U-238	Ispra	32.59%	37.78%	-20.44%
U-236/Total U(RateOfWeight)	Karlsruhe	-13.86%	-10.95%	13.12%
U-236/Total U(RateOfWeight)	Ispra	-13.30%	-10.37%	13.86%
U-236/U-238	Karlsruhe	-13.58%	-10.60%	12.98%
U-236/U-238	Ispra	-13.30%	-10.31%	13.35%
U-238/Total U(RateOfWeight)	Karlsruhe	-0.31%	-0.37%	0.14%
U-238/Total U(RateOfWeight)	Ispra	-0.31%	-0.37%	0.14%

Table 5-13. B4 fuel element at 268 cm percent differences between SFCOMPO values and PENBURN burnup results (SFCOMPO reports 22.3 GWD/MTU)

Data Type	SFCOMPO Values	Percent Differences		
		initial-xs	burnup-xs	burnup-xs
		.339 g/cc	.339 g/cc	.445 g/cc
Cs-137/U-238	1.57E-03	-84.81%	-77.45%	-75.52%
Nd-148/U-238	4.22E-04	-83.21%	-76.95%	-75.08%
Pu-239/Total Pu(RateOfWeight)	6.24E-01	30.49%	34.14%	23.03%
Pu-239/U-238	5.24E-03	23.30%	29.21%	19.65%
Pu-240/Pu-239	3.68E-01	-78.21%	-69.68%	-52.78%
Pu-240/Total Pu(RateOfWeight)	2.29E-01	-71.49%	-59.21%	-41.75%
Pu-241/Pu-239	1.46E-01	-8.78%	-48.14%	-23.63%
Pu-241/Total Pu(RateOfWeight)	1.07E-01	1.35%	-40.77%	-20.00%
Pu-242/Pu-239	4.66E-02	-68.42%	-84.11%	-62.89%
Pu-242/Total Pu(RateOfWeight)	2.89E-02	-58.54%	-78.56%	-54.06%
Total Pu/Total U	8.30E-03	-5.94%	-4.17%	-2.74%
U-235/Total U(RateOfWeight)	9.35E-03	43.46%	49.00%	-13.69%
U-235/U-238	9.60E-03	42.01%	47.58%	-14.95%
U-236/Total U(RateOfWeight)	3.12E-03	-14.91%	-12.04%	11.72%
U-236/U-238	3.19E-03	-15.42%	-12.51%	10.55%
U-238/Total U(RateOfWeight)	9.88E-01	-0.41%	-0.47%	0.04%

Table 5-14. C5 fuel element at 268 cm percent differences between SFCOMPO values and PENBURN burnup results (SFCOMPO reports 23.0 GWD/MTU)

Data Type	SFCOMPO Values	Percent Difference		
		initial-xs .339 g/cc	burnup-xs .339 g/cc	burnup-xs .445 g/cc
Cs-137/U-238	1.78E-03	-86.60%	-80.10%	-78.40%
Kr-84/Kr-83	2.49E+00	-97.71%	-97.83%	-97.07%
Nd-148/U-238	4.36E-04	-83.75%	-77.69%	-75.88%
Pu-239/Total Pu(RateOfWeight)	6.07E-01	33.97%	37.74%	26.27%
Pu-239/U-238	5.12E-03	25.96%	32.03%	22.17%
Pu-240/Pu-239	3.97E-01	-79.67%	-71.71%	-55.94%
Pu-240/Total Pu(RateOfWeight)	2.41E-01	-72.77%	-61.04%	-44.37%
Pu-241/Pu-239	1.56E-01	-14.05%	-51.13%	-28.05%
Pu-241/Total Pu(RateOfWeight)	1.09E-01	0.03%	-41.52%	-21.08%
Pu-242/Pu-239	5.36E-02	-72.15%	-86.00%	-67.26%
Pu-242/Total Pu(RateOfWeight)	3.25E-02	-62.65%	-80.70%	-58.62%
Total Pu/Total U	8.37E-03	-6.77%	-5.01%	-3.62%
U-235/Total U(RateOfWeight)	8.96E-03	49.08%	54.93%	-10.73%
U-235/U-238	9.05E-03	50.00%	55.98%	-10.59%
U-236/Total U(RateOfWeight)	3.29E-03	-19.16%	-16.46%	6.03%
U-236/U-238	3.32E-03	-18.58%	-15.81%	6.30%
U-238/Total U(RateOfWeight)	9.88E-01	-0.41%	-0.47%	0.05%

Table 5-15. E3 fuel element at 268 cm percent differences between SFCOMPO values and PENBURN burnup results (SFCOMPO reports 23.5 GWD/MTU)

Data Type	SFCOMPO Values	Percent Difference		
		initial-xs	burnup-xs	burnup-xs
		.339 g/cc	.339 g/cc	.445 g/cc
Cs-137/U-238	1.59E-03	-84.99%	-77.73%	-75.82%
Nd-148/U-238	4.58E-04	-84.53%	-78.77%	-77.04%
Pu-239/Total Pu(RateOfWeight)	6.15E-01	32.23%	35.95%	24.63%
Pu-239/U-238	5.02E-03	28.47%	34.66%	24.61%
Pu-240/Pu-239	3.82E-01	-78.87%	-70.60%	-54.21%
Pu-240/Total Pu(RateOfWeight)	2.35E-01	-72.07%	-60.05%	-42.95%
Pu-241/Pu-239	1.50E-01	-10.62%	-49.17%	-25.18%
Pu-241/Total Pu(RateOfWeight)	1.08E-01	440.44%	260.10%	241.07%
Pu-242/Pu-239	5.05E-02	-70.45%	-85.14%	-65.26%
Pu-242/Total Pu(RateOfWeight)	3.10E-02	-60.85%	-79.76%	-56.62%
Total Pu/Total U	8.07E-03	-3.30%	-1.48%	-0.03%
U-235/Total U(RateOfWeight)	9.03E-03	47.93%	53.70%	-11.43%
U-235/U-238	9.14E-03	48.53%	54.42%	-11.48%
U-236/Total U(RateOfWeight)	3.27E-03	-18.66%	-15.94%	6.68%
U-236/U-238	3.31E-03	-18.33%	-15.55%	6.62%
U-238/Total U(RateOfWeight)	9.88E-01	-0.41%	-0.47%	0.05%

Table 5-16. E5 fuel element at 268 cm percent differences between SFCOMPO values and PENBURN burnup results(SFCOMPO reports 25.2 GWD/MTU)

Data Type	Measurement Laboratory	Percent Difference		
		initial-xs	burnup-xs	burnup-xs
		.339 g/cc	.339 g/cc	.445 g/cc
Cs-134/Cs-137 (Ratio of Activity)	Ispra	-93.19%	-93.17%	-93.18%
Cs-137/U-238	Karlsruhe	-87.23%	-81.04%	-79.44%
Cs-137/U-238	Ispra	-86.58%	-80.08%	-78.40%
Eu-154/Cs-137 (Ratio of Activity)	Ispra	-99.61%	-99.59%	-99.64%
Nd-148/U-238	Karlsruhe	-85.59%	-80.23%	-78.63%
Pu-239/Total Pu(RateOfWeight)	Karlsruhe	42.94%	47.06%	34.68%
Pu-239/Total Pu(RateOfWeight)	Ispra	42.19%	46.28%	33.97%
Pu-239/U-238	Karlsruhe	38.08%	44.83%	33.84%
Pu-239/U-238	Ispra	35.75%	42.38%	31.58%
Pu-240/Pu-239	Karlsruhe	-82.44%	-75.58%	-61.99%
Pu-240/Pu-239	Ispra	-82.44%	-75.58%	-61.99%
Pu-240/Total Pu(RateOfWeight)	Karlsruhe	-74.92%	-64.12%	-48.85%
Pu-240/Total Pu(RateOfWeight)	Ispra	-74.72%	-63.85%	-48.46%
Pu-241/Pu-239	Karlsruhe	-22.09%	-55.71%	-34.91%
Pu-241/Pu-239	Ispra	-23.84%	-56.70%	-36.36%
Pu-241/Total Pu(RateOfWeight)	Karlsruhe	-3.07%	-43.30%	-23.70%
Pu-241/Total Pu(RateOfWeight)	Ispra	-2.21%	-42.80%	-23.02%
Pu-242/Pu-239	Karlsruhe	-79.35%	-89.64%	-75.79%
Pu-242/Pu-239	Ispra	-79.55%	-89.74%	-76.02%
Pu-242/Total Pu(RateOfWeight)	Karlsruhe	-70.44%	-84.74%	-67.35%
Pu-242/Total Pu(RateOfWeight)	Ispra	-69.94%	-84.49%	-66.80%
Total Pu/Total U	Karlsruhe	-4.34%	-2.53%	-1.13%
Total Pu/Total U	Ispra	-5.27%	-3.48%	-2.09%
U-235/Total U(RateOfWeight)	Karlsruhe	84.11%	91.52%	8.99%
U-235/Total U(RateOfWeight)	Ispra	88.85%	96.45%	11.79%
U-235/U-238	Karlsruhe	85.28%	92.86%	9.17%
U-235/U-238	Ispra	90.00%	97.77%	11.95%
U-236/Total U(RateOfWeight)	Karlsruhe	-23.40%	-20.91%	0.18%
U-236/Total U(RateOfWeight)	Ispra	-21.38%	-18.82%	2.84%
U-236/U-238	Karlsruhe	-22.83%	-20.27%	0.47%
U-236/U-238	Ispra	-21.03%	-18.41%	2.81%
U-238/Total U(RateOfWeight)	Karlsruhe	-0.50%	-0.56%	-0.03%
U-238/Total U(RateOfWeight)	Ispra	-0.60%	-0.66%	-0.13%

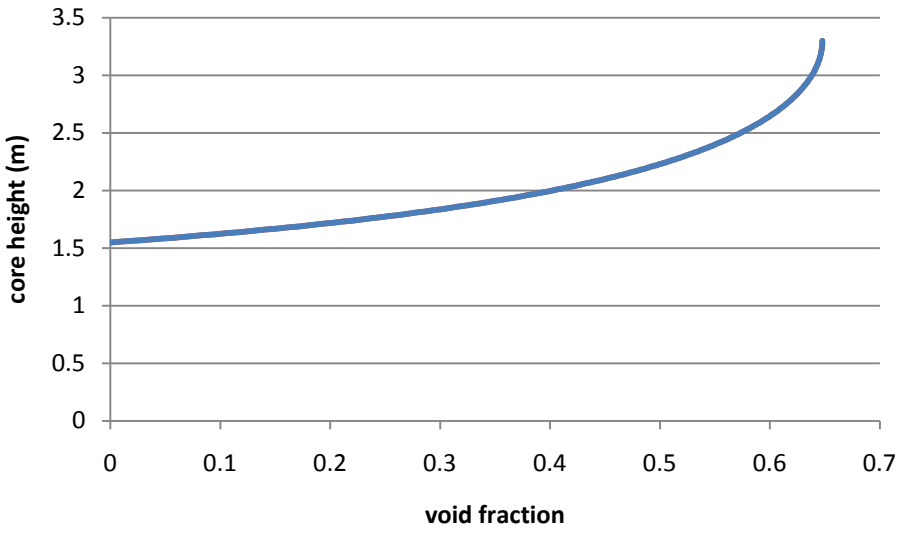

Figure 5-1. Gundremmingen void fraction distribution.

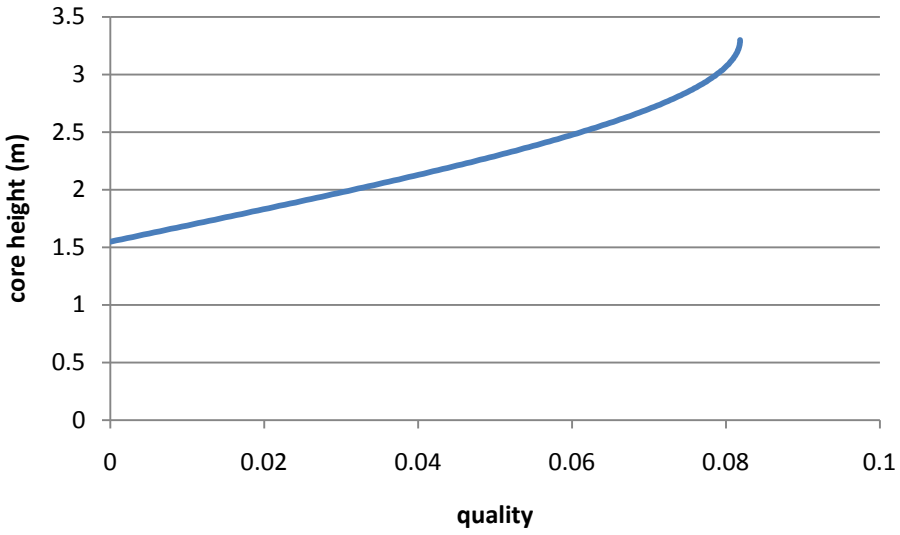

Figure 5-2. Gundremmingen axial quality.

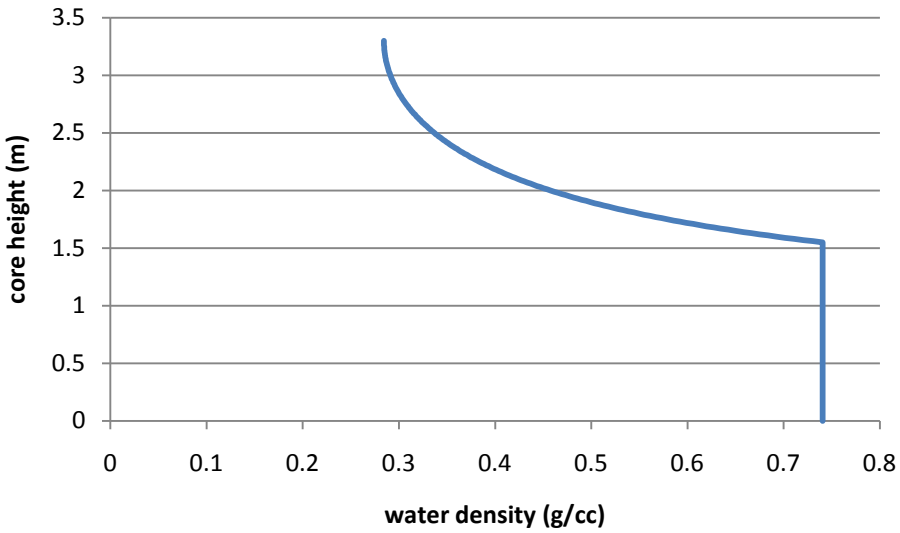

Figure 5-3. Gundremmingen water density.

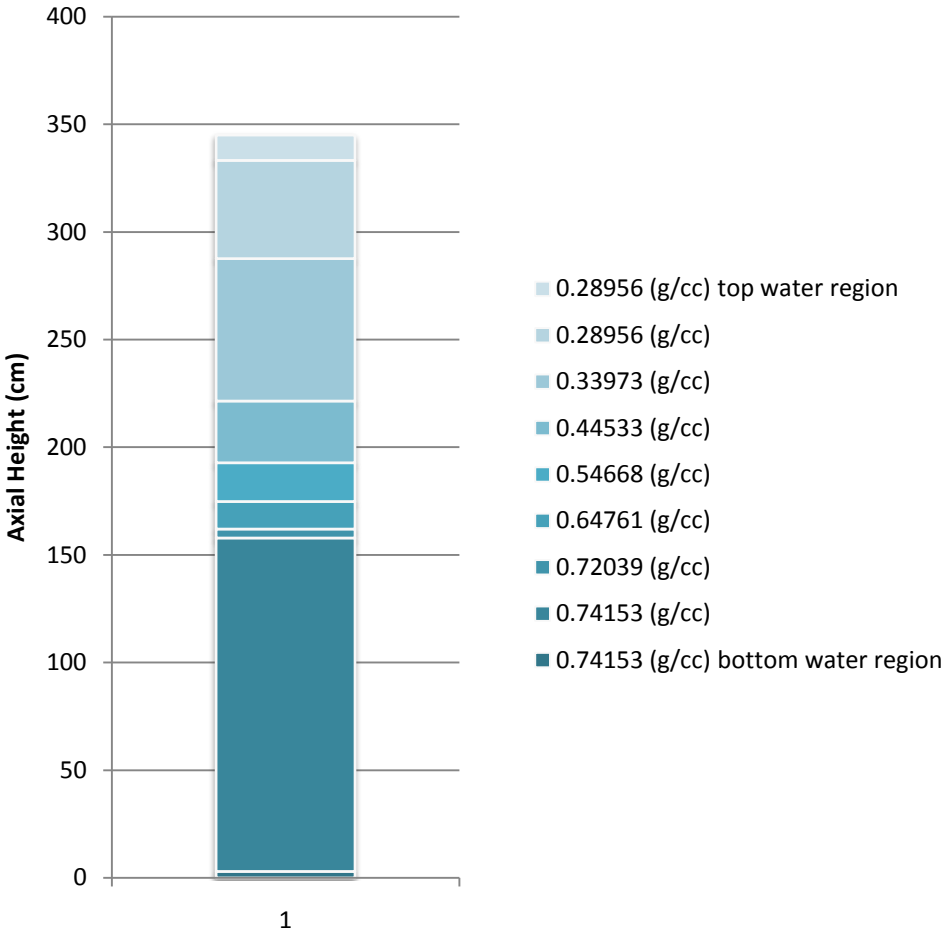

Figure 5-4. Gundremmingen BWR axial zone partitioning.

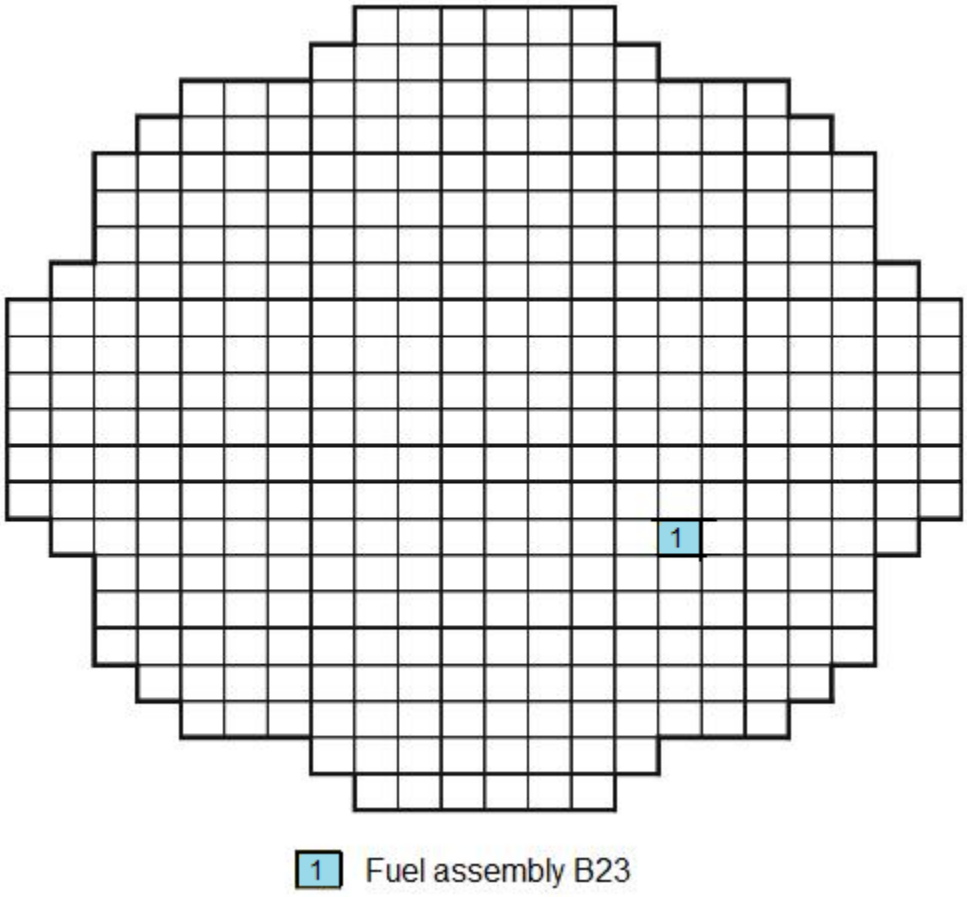

Figure 5-5. Gundremmingen B23 assembly location in core.

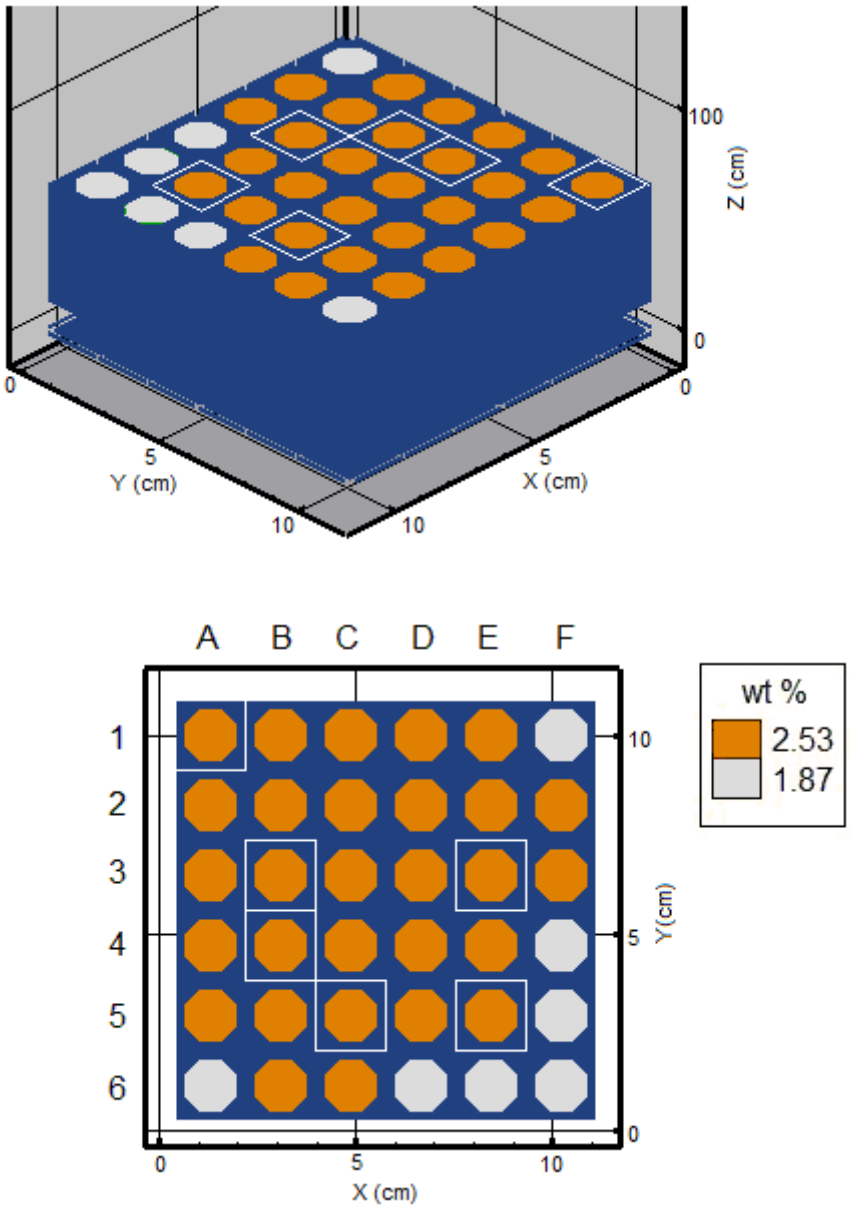

Figure 5-6. Gundremmingen B23 assembly enrichments and sampling positions.

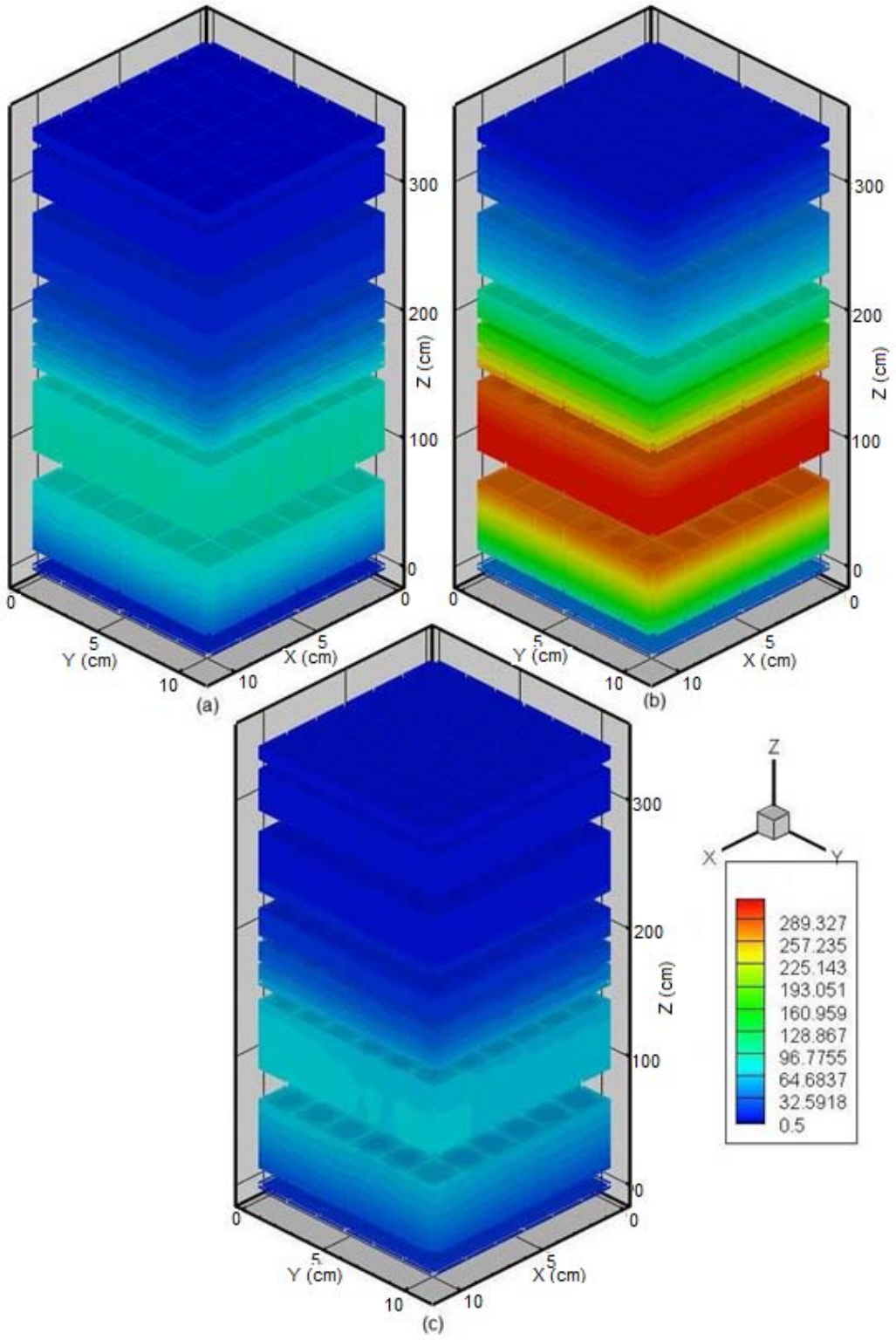

Figure 5-7. Gundremmingen B23 assembly relative fluxes (0.00 GWD/MTU) for (a) group 1 (b) group 2 (c) group 3 [PENTRAN code run, 16 processors (4 in angle, 1 in energy, 4 in space),cross sections with a P_1 Legendre order, S_8 quadrature, specular reflective boundary conditions in x-y direction, vacuum boundaries in ± z directions].

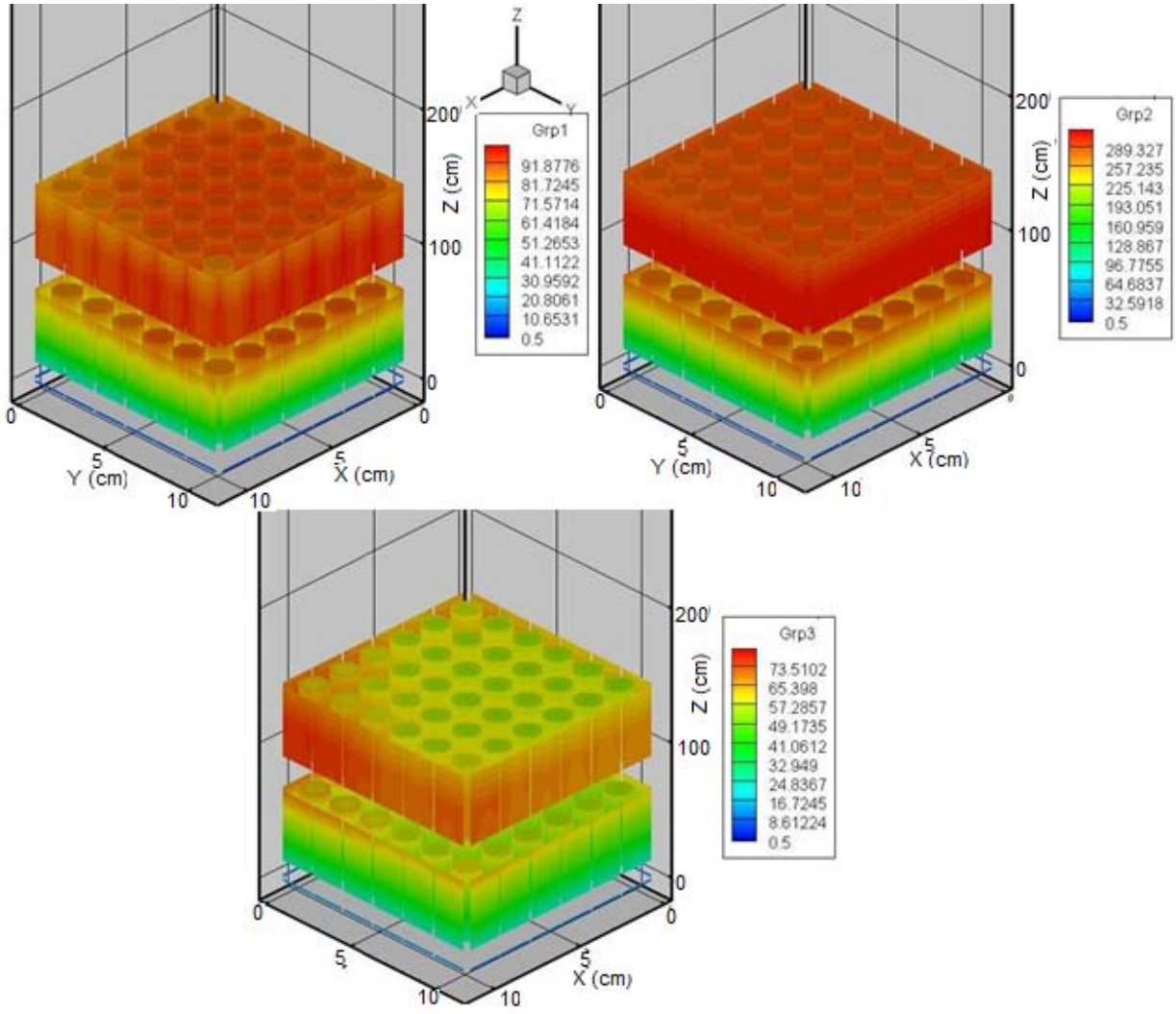

Figure 5-8. Gundremmingen B23 assembly relative group fluxes (0.00 GWD/MTU) [PENTRAN code run, 16 processors (4 in angle, 1 in energy, 4 in space),cross sections with a P_1 Legendre order, S_8 quadrature, specular reflective boundary conditions in x-y direction, vacuum boundaries in ± z directions].

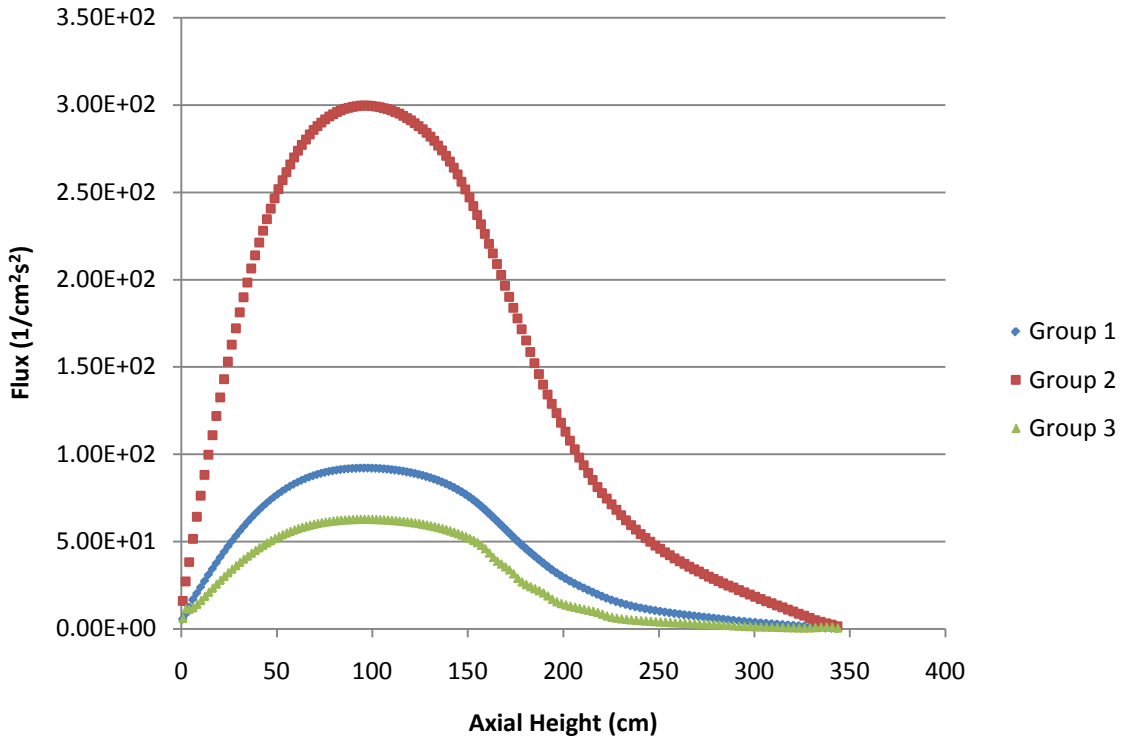

Figure 5-9. Gundremmingen B23 assembly relative group fluxes (0.00 GWD/MTU).

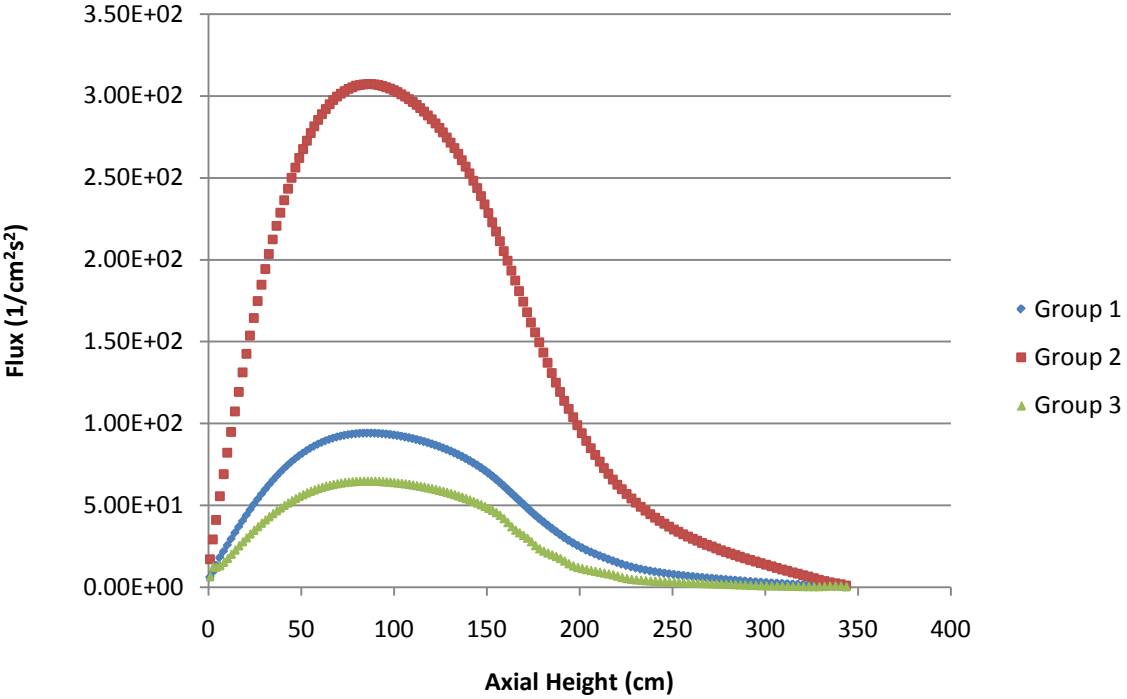

Figure 5-10. Gundremmingen B23 assembly relative group fluxes (0.06 GWD/MTU).

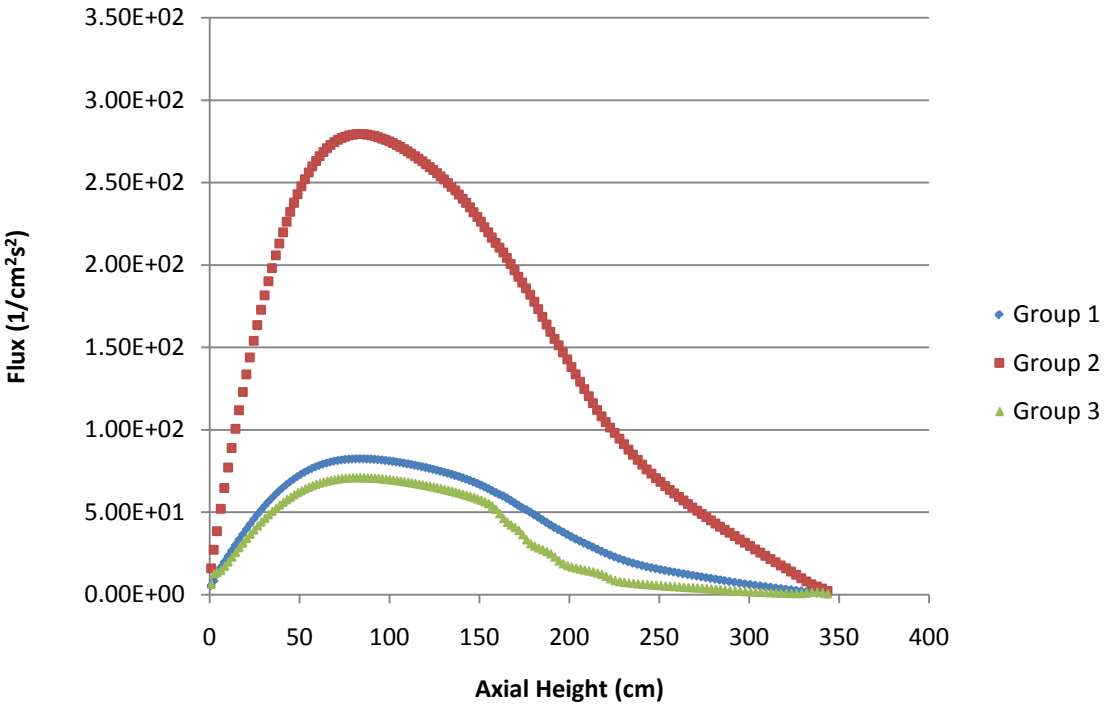

Figure 5-11. Gundremmingen B23 assembly relative group fluxes (3.74 GWD/MTU).

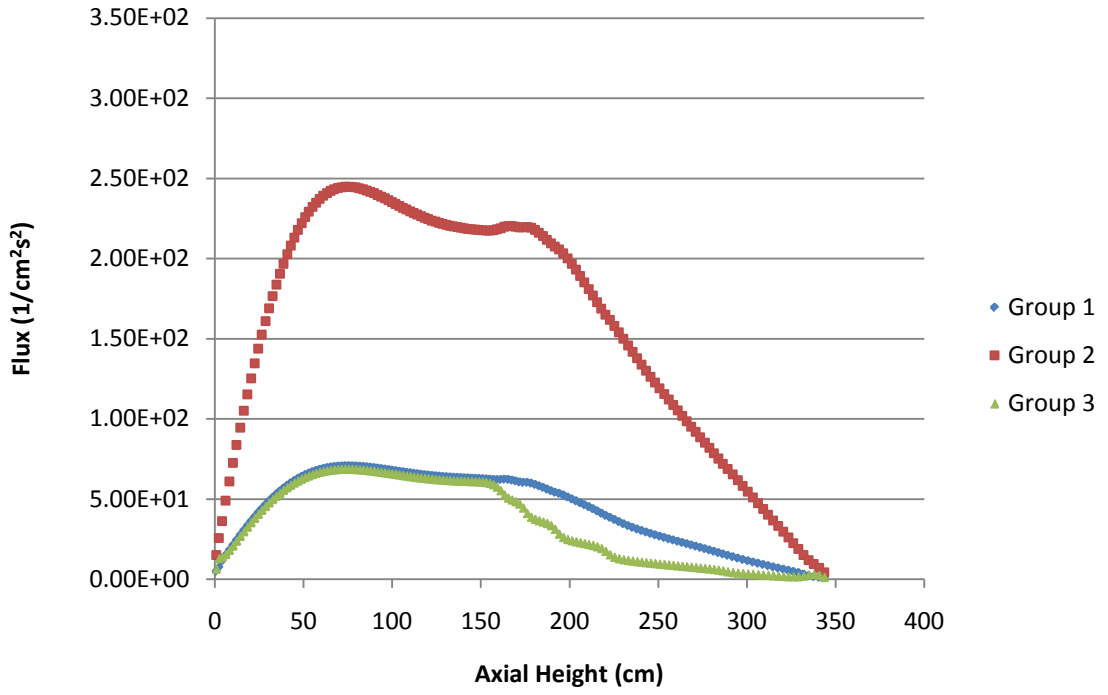

Figure 5-12. Gundremmingen B23 assembly relative group fluxes (5.83 GWD/MTU).

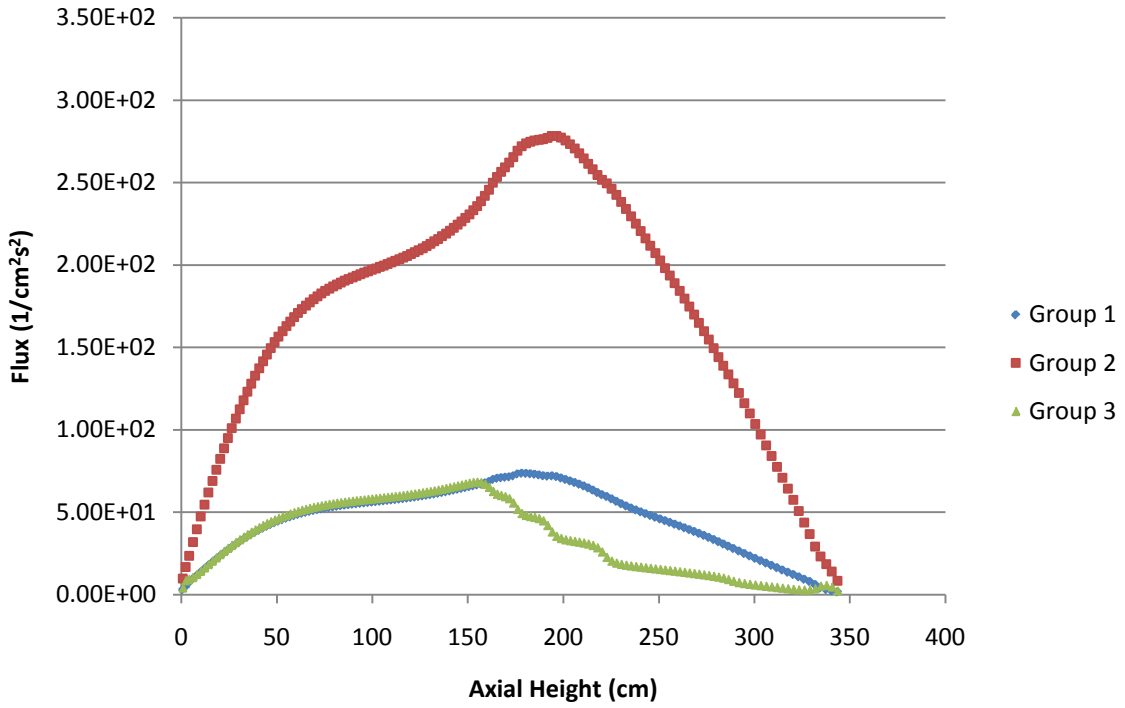

Figure 5-13. Gundremmingen B23 assembly relative group fluxes (7.73 GWD/MTU).

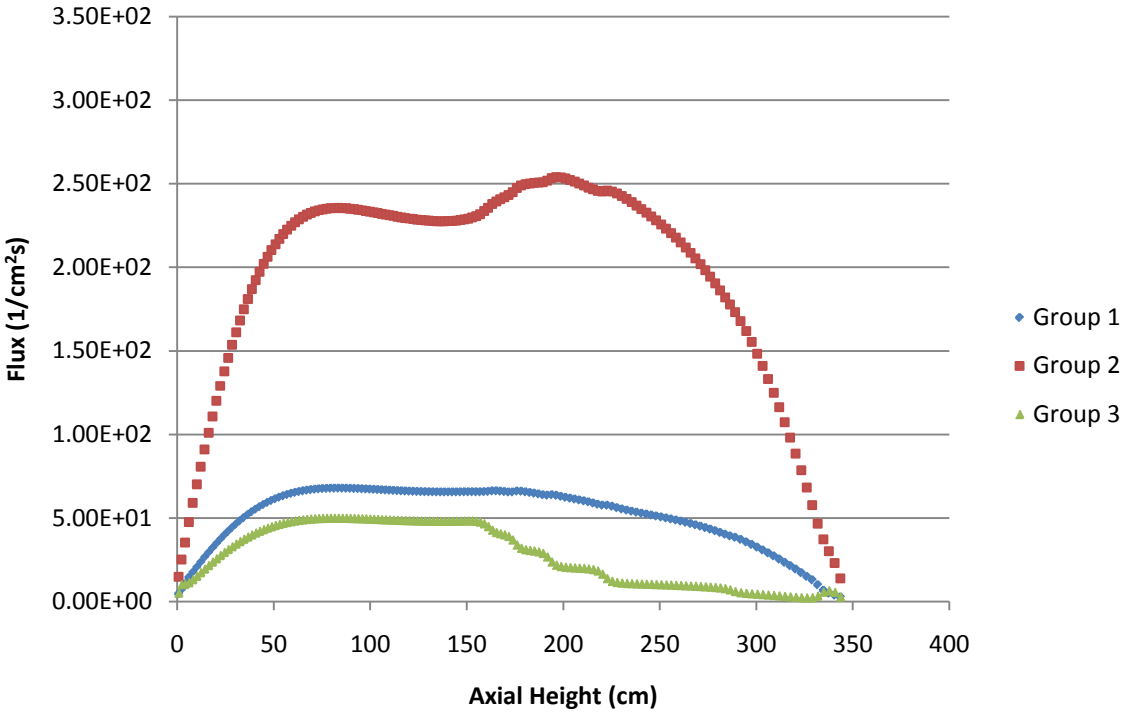

Figure 5-14. Gundremmingen B23 assembly relative group fluxes (19.12 GWD/MTU).

CHAPTER 6
CONCLUSIONS AND FUTURE WORK

Key findings in this study include the need to move from 2-D deterministic Sn transport analysis to 3-D analysis for boiling water systems, especially when performing burnup studies in boiling water reactors to account for the impact different axial densities have on the overall isotopic results. The use of 3-D deterministic transport codes is also useful when performing fixed source analyses to determine the detector range for novel detector concepts, in addition to optimal positioning of the detectors.

Major contributions overall include modifying the multigroup cross section generation procedure to account for multiple cross sections for the same nuclide depending on material region. The XSMERGE code was developed to sort and group nuclides prior to using GMIX which converts the microscopic cross section data to macroscopic data used by PENTRAN. A void fraction distribution solver was also created to determine the axial void distribution in a boiling water reactor assembly when provided with six operating parameters and initially assuming sinusoidal heat generation. And finally the FSPREP program was developed to automatically render the fixed source for a problem set-up when performing a forward transport calculation. The detector response was calculated from both the forward and adjoint transport calculations, with the adjoint transport calculation providing the detector range for the SiC semiconductor detector. The neutron response contribution from the thermal, epithermal and fast group was 72%, 27% and 1% respectively.

Implementing a procedure to develop cross sections for a boiling water reactor fuel assembly and using the changing void fraction in the assembly displayed the need to use 3-D models when analyzing BWRs. The shifting flux after 3.74 GWD/MTU presented further advancement possibilities for the BWR model including creating a coupled thermal hydraulics

and transport solver driver when performing burnup calculations. PENBURN burnup results displayed better agreement with a water density of 0.44 g/cm^3 at 268 cm as opposed to 0.366 g/cm^3.

The multigroup cross section generation procedure using SCALE 5.1 did not allow for more than two lattice cell calculations within a single SCALE run due to memory allocation issues. Due to computer requirements when generating the multigroup cross sections, a single lattice cell calculation was performed at each water density chosen and then the microscopic cross sections were combined and sorted. Initially a minimum number of water densities was utilized in order to decrease the amount of computations required to generate the multigroup cross section data, however, the seven different axial water density zones may not be sufficient to represent a BWR assembly when performing burnup calculations. The Pu series experienced a significant impact when dealing with different water densities around the fuel, even with a density delta of 0.1 g/cm^3. Moving from a water density of 0.33 g/cm^3 to 0.445 g/cm^3 resulted in a 15% difference for the Pu-240 amount, 16% for Pu-241, and 13% for Pu-242. When the water density was 0.647 g/cm^3 instead of 0.546 g/cm^3 there was a difference of 29% for Pu-240, 19% for Pu-241, and 33% for Pu-242. These large changes in isotopic compositions with a water density change of only 0.1 g/cm^3 indicates the need to include more water densities so that the change between regions is not as large.

These small changes in water density have a large impact in burnup calculations that can be minimized if there are more water densities for the BWR model. Future BWR assembly models should include more than seven water density regions with a maximum delta between water densities of 0.025 g/cm^3. Calculating the optimum number of water densities adequate for all burnup points an assembly undergoes is an area of future work. The need to significantly

increase the number of water regions requires the development of a driver to automatically perform the DEV-XS procedure especially when generating a BWR cross section library data set.

Another area of improvement comes in regard to control rod positioning. Since control rod use history is not readily available for the BWRs listed in the SFCOMPO database, creating another case that implements the use of a control rod and analyzing the impact it has on the burnup results can be investigated. Modeling additional BWRs in the SFCOMPO database that include fuel rods containing gadolinium is future work for code validation and developing multigroup cross section data for this fuel type.

APPENDIX A
SCALE 5.1 SAMPLE INPUT FILE

```
'BWR Fuel Pin cross section development 1st moderator density 0.74153
'
'start tnewt control sequence
=t-newt    parm=(addnux=3)
'
'title card
BWR homogenized pin 2.53 wtp enriched 1st moderator density 0.74153
'
'calling the 238 fine group ENDF-B6 library
V6-238
'
'initiate composition read
read comp
' UO2 fuel-specifications for 2.53 wtp BWR fuel pin from Gundremmingen 6x6 BWR
WTPThomg1 11 9.23798115   16   8016  9.89770683
                          92234 0.01692995
                          92235 1.86229452
                          92236 0.008833017
                          92238 71.7204216
                          2004  0.025670946
                          40000 16.4681431
'Following nuclides are added in trace quantities in order to produce on output collapsed XS file
                         92237 1E-5
                         93238 1E-5 93239 1E-5
                         94236 1E-5 94244 1E-5
                         96245 1E-5 96246 1E-5 96247 1E-5
                         61601 1E-5                        1 923.   end
WTPTh2o_1 41 0.74153  2 1001 11.189
                   8016 88.811                           1  539.   end
'
end comp
'
'read celldata initiation statement
read celldata
'
'geometry type and boundary conditions
'note that here we must define an approximation for a unit cell calculations within the cross
section card
'
latticecell squarepitch pitch 1.78 41 fueld 1.428  11  end
'
'end of celldata parameters'
end celldata
'
```

```
'
READ model
BWR Pin
READ param
run=yes
collapse=yes
sn=8
epsilon=1e-5
echo=yes
drawit=yes
inners=10
prtmxsec=yes
prtmxtab=yes
prtxsec=yes
prtbroad=yes
END param
READ collapse
22r1 177r2 39r3
END collapse
READ materials
11 1 'homg1' end
41 1 'h2o' end
END materials
READ geom
' homogenized BWR pin 2.53 wt%
global unit 1
cylinder 10 0.714
cuboid 20 4p0.89
media 11 1 10
media 41 1 20 -10
boundary 20 11 11
END geom
'
'start reading bounds'
READ bounds
'
'all boundaries are reflective boundary condition'
-x=reflective +x=reflective -y=reflective +y=reflective
END bounds
END model
'end of tnewt sequence
END
'
=alpo
'  textoutp    notused
0$$  7          0
```

```
' wrklibs  iht  ihs  ihm  Pnord PrtGA PrtScm  NoCorr
1$$ 1      3    4   6    1     0      0      0    0 T
' wrklin# Accept
2$$ 30     0    T
end
=shell
copy _pun0000 "%RTNDIR%\water1XS"
```

APPENDIX B
FSPREP SAMPLE INPUT

```
/Number of energy groups
3
/File names for the source for each energy group
whasm1.src
whasm2.src
whasm3.src
/nsdef variable in block 5 of PENTRAN input deck
27
/nscmsh variable in block 5 of PENTRAN input deck
6 7 8 10
11 12 14
15 16 22
23 24 26
27 28 30
31 32 38
39 40 42
43 44 46
47 48
```

APPENDIX C
FSPREP SAMPLE OUTPUT

```
1 1 3888
 75R0.00000E+00  0.58374E+01  0.57748E+01  0.57582E+01
   0.57482E+01   0.57673E+01   0.58189E+01  6R0.00000E+00
   0.58081E+01   0.57532E+01   0.57389E+01   0.57348E+01
   0.57573E+01   0.58108E+01  6R0.00000E+00   0.58277E+01
   0.57748E+01   0.57600E+01   0.57604E+01   0.57832E+01
   0.58392E+01  5R0.00000E+00   0.58373E+01   0.57408E+01
   0.56839E+01   0.56555E+01   0.56539E+01   0.56727E+01
   0.57231E+01   0.58085E+01  4R0.00000E+00   0.58006E+01
   0.57154E+01   0.56618E+01   0.56389E+01   0.56407E+01
   0.56624E+01   0.57175E+01   0.58041E+01  4R0.00000E+00
   0.58176E+01   0.57350E+01   0.56825E+01   0.56621E+01
   0.56640E+01   0.56887E+01   0.57465E+01   0.58348E+01
.
.
.
```

APPENDIX D
ALPO INPUT MODIFICATION FOR XSMCNP

```
=alpo
'  textoutp    notused
0$$  7          0
'  wrklibs  iht  ihs  ihm  Pnord PrtGA PrtScm  NoCorr
1$$  1       5    6   8    1      0      0      0    0 T
'  wrklin# Accept
2$$  30     0    T
end
=shell
copy _pun0000 "%RTNDIR%\water1XS"
end
```

APPENDIX E
MCNP INPUT FILE

```
Homogenized Fuel Gundremmingen BWR Assembly
c cell cards
1    8   1.0 (21 -23 22 -24 4 -5) imp:n=1
2    1   1.0    -3        u=3   imp:n=1   $fuel+gap+clad homogenized
3    8   1.0   3        u=3   imp:n=1   $moderator 0.74153 g/cc
4    0      -8 7 -10 9 lat=1  u=1   imp:n=1 fill=0:5 0:5 0:0 $lattice
              3 3 3 3 3 3
              3 3 3 3 3 3
              3 3 3 3 3 3
              3 3 3 3 3 3
              3 3 3 3 3 3
              3 3 3 3 3 3
5    0        7 -12 9 -14 5 -6     imp:n=1 fill=1
6    2   1.0   -3          u=4   imp:n=1   $fuel+gap+clad homogenized
7    9   1.0  3          u=4   imp:n=1   $moderator 0.72039 g/cc
8   0      -8 7 -10 9  lat=1   u=11  imp:n=1 fill=0:5 0:5 0:0 $lattice
              4 4 4 4 4 4
              4 4 4 4 4 4
              4 4 4 4 4 4
              4 4 4 4 4 4
              4 4 4 4 4 4
              4 4 4 4 4 4
9   0        7 -12 9 -14 6 -15      imp:n=1 fill=11
10    3   1.0   -3         u=5   imp:n=1   $fuel+gap+clad homogenized
11   10  1.0  3         u=5   imp:n=1   $moderator 0.64761 g/cc
12   0     -8 7 -10 9  lat=1  u=21  imp:n=1 fill=0:5 0:5 0:0 $lattice
              5 5 5 5 5 5
              5 5 5 5 5 5
              5 5 5 5 5 5
              5 5 5 5 5 5
              5 5 5 5 5 5
              5 5 5 5 5 5
13   0        7 -12 9 -14 15 -16   imp:n=1 fill=21
14   4   1.0   -3          u=6   imp:n=1   $fuel+gap+clad homogenized
15   11  1.0  3          u=6   imp:n=1   $moderator 0.54668 g/cc
16   0      -8 7 -10 9 lat=1   u=31  imp:n=1 fill=0:5 0:5 0:0 $lattice
              6 6 6 6 6 6
              6 6 6 6 6 6
              6 6 6 6 6 6
              6 6 6 6 6 6
              6 6 6 6 6 6
              6 6 6 6 6 6
17   0        7 -12 9 -14 16 -17    imp:n=1 fill=31
```

```
18   5   1.0    -3        u=7   imp:n=1   $fuel+gap+clad homogenized
19   12  1.0   3        u=7   imp:n=1   $moderator 0.44533 g/cc
20   0     -8 7 -10 9  lat=1  u=41  imp:n=1 fill=0:5 0:5 0:0 $lattice
             7 7 7 7 7 7
             7 7 7 7 7 7
             7 7 7 7 7 7
             7 7 7 7 7 7
             7 7 7 7 7 7
             7 7 7 7 7 7
21   0        7 -12 9 -14 17 -18   imp:n=1 fill=41
22   6   1.0 -3           u=8   imp:n=1   $fuel+gap+clad homogenized
23   13  1.0  3          u=8   imp:n=1   $moderator 0.33973 g/cc
24   0     -8 7 -10 9  lat=1   u=51  imp:n=1 fill=0:5 0:5 0:0 $lattice
             8 8 8 8 8 8
             8 8 8 8 8 8
             8 8 8 8 8 8
             8 8 8 8 8 8
             8 8 8 8 8 8
             8 8 8 8 8 8
25   0        7 -12 9 -14 18 -19    imp:n=1 fill=51
26   7   1.0 -3           u=9   imp:n=1   $fuel+gap+clad homogenized
27   14  1.0  3          u=9   imp:n=1   $moderator 0.28956 g/cc
28   0       -8 7 -10 9    lat=1 u=61   imp:n=1 fill=0:5 0:5 0:0 $lattice
             9 9 9 9 9 9
             9 9 9 9 9 9
             9 9 9 9 9 9
             9 9 9 9 9 9
             9 9 9 9 9 9
             9 9 9 9 9 9
29   0        7 -12 9 -14 19 -20       imp:n=1 fill=61
30   14   1.0 (21 -23 22 -24 20 -25) imp:n=1
31   15   1.0  (21 -23 22 -24 5 -20) (-7:12:-9:14)  imp:n=1
77   0       -4:25:-21:23:-22:24         imp:n=0

c surface cards
3    c/z 0.89 0.89 0.714
*4    pz  0.00                $ -z plane fuel pin and assembly
5    pz  3
6    pz  157.9176              $  z plane fuel pin and assembly
7    px  0.00
8    px  1.78
9    py  0.00
10    py  1.78
c assembly outer volume
12   px  10.68
14   py  10.68
```

```
c axial z
15   pz  162.1
16   pz  174.8
17   pz  192.8
18   pz  221.4
19   pz  287.6
20   pz  333.2
c zircaloy channel enclosing assembly
*21   px  -0.25
*22   py  -0.25
*23   px  10.93
*24   py  10.93
*25   pz 345

c data cards
mode n
f4:n   5
f14:n  9
f24:n  13
f34:n  17
f44:n  21
f54:n  25
f64:n  29
m1  1000.22m  1.0
m2  2000.22m  1.0
m3  3000.22m  1.0
m4  4000.22m  1.0
m5  5000.22m  1.0
m6  6000.22m  1.0
m7  7000.22m  1.0
m8  8000.22m  1.0
m9  9000.22m  1.0
m10  10000.22m  1.0
m11  11000.22m  1.0
m12  12000.22m  1.0
m13  13000.22m  1.0
m14  14000.22m  1.0
m15  15000.22m 1.0
mt1 lwtr.60t
mt2 lwtr.60t
mt3 lwtr.60t
mt4 lwtr.60t
mt5 lwtr.60t
mt6 lwtr.60t
mt7 lwtr.60t
c
```

```
e0     6.250E-07  1.010E+00  2.000E+01
c
mgopt f 3
kcode   50000 1.00 200 1000
ksrc    0.89 0.89 5
        2.67 0.89 5
        4.45 0.89 5
        6.23 0.89 5
        8.01 0.89 5
        9.79 0.89 5
        0.89 2.67 5
        2.67 2.67 5
        4.45 2.67 5
.
.
.
```

APPENDIX F
SCALE 5.1 T-DEPL INPUT

```
'BWR Fuel Pin cross section development 1st moderator density 0.74153
'
'start tnewt control sequence
=t-depl    parm=(savlib,addnux=3)
'
'title card
BWR homogenized pin 2.53 wtp enriched 1st moderator density 0.74153
'
'calling the 238 fine group ENDF-B6 library
V6-238
'
'initiate composition read
read comp
' UO2 fuel-specifications for 2.53 wtp BWR fuel pin from Gundremmingen 6x6 BWR
WTPThomg1 11 9.23798115   16   8016  9.89770683
                        92234 0.01692995
                        92235 1.86229452
                        92236 0.008833017
                        92238 71.7204216
                        2004  0.025670946
                        40000 16.4681431
'Following nuclides are added in trace quantities in order to produce on output collapsed XS file
                      92237 1E-5
                      93238 1E-5 93239 1E-5
                      94236 1E-5 94244 1E-5
                      96245 1E-5 96246 1E-5 96247 1E-5
                      61601 1E-5                        1 900.   end
WTPTh2o_1 41 0.74153  2 1001 11.189
                   8016 88.811                          1  500.   end
'
end comp
'
'read celldata initiation statement
read celldata
'
'geometry type and boundary conditions
'note that here we must define an approximation for a unit cell calculations within the cross
section card
'
latticecell squarepitch pitch 1.78 41 fueld 1.428  11  end
'
'end of celldata parameters'
end celldata
```

```
READ burndata
 p=23.0 b=40.0  d=0.0     end
 p=23.0 b=300.0 d=0.0    end
 p=23.0 b=300.0 d=0.0     end
 p=23.0 b=272.0 d=0.0     end
 p=23.0 b=200.0 d=0.0     end
 p=23.0 b=68.0 d=0.0     end
END burndata
READ depletion
-11
END depletion
'
'
READ model
BWR Pin
READ param
run=yes
collapse=yes
sn=8
epsilon=1e-5
echo=yes
drawit=yes
inners=10
prtmxsec=yes
prtmxtab=yes
prtxsec=yes
prtbroad=yes
END param
READ collapse
22r1 177r2 39r3
END collapse
READ materials
11 1 'homg1' end
41 1 'h2o' end
END materials
READ geom
' homogenized BWR pin 2.53 wt%
global unit 1
cylinder 10 0.714
cuboid 20 4p0.89
media 11 1 10
media 41 1 20 -10
boundary 20 19 19
END geom
'
'start reading bounds'
```

```
READ bounds
'
'all boundaries are reflective boundary condition'
-x=reflective +x=reflective -y=reflective +y=reflective
END bounds
END model
'end of tdepl sequence
END
'
=shell
copy savcol00 "%RTNDIR%\savcol00"
copy savcol01 "%RTNDIR%\savcol01"
copy savcol02 "%RTNDIR%\savcol02"
copy savcol03 "%RTNDIR%\savcol03"
copy savcol04 "%RTNDIR%\savcol04"
copy savcol05 "%RTNDIR%\savcol05"
copy savcol06 "%RTNDIR%\savcol06"
end
```

APPENDIX G
ALPO INPUT FOR COLLAPSED CROSS SECTION FILE

```
=shell
copy "C:\Users\mrowe\Desktop\bwr burnup xsc\1\fueltemp900\savcol00" "%TMPDIR%\ft40f001"
end
=alpo
'  textoutp    notused
0$$   7           0
'  wrklibs  iht  ihs  ihm  Pnord PrtGA PrtScm  NoCorr
1$$   1      3    4   6    1      0      0      0    0 T
'  wrklin# Accept
2$$     40    0    T
end
=shell
copy "_pun0000" "%RTNDIR%\water1t_3_0"
end
```

APPENDIX H
BURNSET INPUT FILE

```
/ problem name | predictor corrector flag ( 0=no, 1=PCA Std., 2=PCA HE) | memory save option (0=inactive, 1=active)
        bwr 0 0
/ # of processors for parallel PENTRAN run | Step 0 flux files exist (0=no, 1=yes) | Restart? ( no-<0, >0-last complete step# folder)
        16 0 -1
        / REPRO flag (1=use preconditioner flux files, 0=no preconditioner flux files) | precflx flag for initial PENTRAN run (0=no, 1=yes)
        1 1
        / INTERPXS flag (1=activate, 0=user supplied .xsc file for entire sequence) | INTERPXS option | Fuel Temp, Mod Temp (K) | INTERPXS optiond data
        1 2 923 574 t
        / PENTRAN Convergence STOP flag [interrupt sequence based on PENTRAN convergence] (0=no, 1=yes)
        0
        / Following 3 lines dedicated to PENPOW Problem Description
          Gundremmingen BWR 6x6 assembly
          Modeled after assembly B23 in SFCOMPO
          7 axial water densities
        / number of fuel materials
        252
        / range of fuel material number: eg. 1 10
        1 252
        / Following 3 lines dedicated to PENBURN Problem Description
          Gundremmingen BWR 6x6 assembly
          Modeled after assembly B23 in SFCOMPO
          7 axial water densities
        / # of irradiation/cool steps
        23
        / power ( (-) indicates Watts/g; (+) indicates Watts), time, time unit, irrad (i)/cool(c), print step, print option, GMIX keyword
        -20.9283 1    d  i 1 2 s1
        -20.9283 1    d  i 1 2 s2
        -20.9283 1    d  i 1 2 s3
        -20.9283 1    d  i 1 2 s4
        -20.9283 3    d  i 1 2 s5
        -20.9283 12   d  i 1 2 s6
        -20.9283 40   d  i 1 2 s7
        -20.9283 40   d  i 1 2 s8
        -20.9283 80   d  i 1 2 s9
        -20.9283 100  d  i 1 2 s10
        0       56   d  c 1 2 s11
        -18.9814 100  d  i 1 2 s12
        -18.9814 100  d  i 1 2 s13
        -18.9814 123  d  i 1 2 s14
        0       33   d  c 1 2 s15
        -18.9069 90   d  i 1 2 s16
        -18.9069 100  d  i 1 2 s17
        -18.9069 100  d  i 1 2 s18
        0       61   d  c 1 2 s19
        -16.7443 100  d  i 1 2 s20
        -16.7443 100  d  i 1 2 s21
```

-16.7443 109 d i 1 2 s22
0 10 d c 1 2 s23

LIST OF REFERENCES

Brown, F.B., Kornreich, D.E., Parson, D.K., and Ueki, T., 2003. Autocorrelation and Dominance Ratio in Monte Carlo Criticality Calculations, Nucl. Sci. Eng, 145, pp.279-290.

DeHart, M.D., Hermann, O.H. 1998. Validation of SCALE (SAS2H) Isotopic Predictions for BWR Spent Fuel. Oak Ridge National Laboratory, Oak Ridge. TN.

DeHart, M. D., 2006a. NEWT: A New Transport Algorithm for Two-Dimensional Discrete Ordinates Analysis in Non-Orthogonal Geometries, SCALE5.1 Manual. Oak Ridge National Laboratory, Oak Ridge, TN.

DeHart, M.D., 2006b. TRITON: A Two-Dimensional Transport and Depletion Module for Characterization of Spent Nuclear Fuel, SCALE5.1 Manual. Oak Ridge National Laboratory, Oak Ridge, TN.

Duderstadt, J.J., Hamilton, L.J., 1976. Nuclear Reactor Analysis, John Wiley & Sons, New York.

Dulloo, A.R., Ruddy, F.H., Seidel, J.G., Adams, J.M., Nico, J.S., and Gilliam, D.M., 2003. The thermal neutron response of miniature silicon carbide semiconductor detectors. Nuclear Instruments and Methods in Physics Research, Volume A 498, pp. 415-423.

Greene, N.M., Dunn, M.E., 2006. User's Guide for AMPX Utility Modules, SCALE5.1 Manual. Oak Ridge National Laboratory, Oak Ridge, TN.

Haghighat, A., Wagner, J.C., 2003. Monte Carlo Variance Reduction with Deterministic Importance Functions, Progress in Nuclear Energy, Vol 42(1).

Hollenbach, D.F., Petrie, L.M., 2006. WORKER: SCALE System Module for Creating and Modifying Working Format Libraries, SCALE5.1 Manual. Oak Ridge National Laboratory, Oak Ridge, TN.

Jatuff, J., Giust, F., Krouthen, J., Helmersson, S., Chawla, R. 2005. Effects of void uncertainties on the void reactivity coefficient and pin power distributions for a 10 x 10 BWR assembly, Annals of Nuclear Energy, Vol 33, pp. 119-125.

Kalos, M. H., Whitlock, P. A. 1986. Monte Carlo Methods. John Wiley & Sons, Inc. Germany.

Kazimi, M. S., Todreas, N. E. 1990. Nuclear Systems I: Thermal Hydraulic Fundamentals. Taylor & Francis Group, LLC, New York.

Khorsandi, B., Fard, M. R., Blue, T. E., Miller, D. W.,Windl, W., 2007. Monte Carlo Modeling of Count Rates and Defects in a Silicon Carbide Detector Neutron Monitor System Highlighting GT-MHR, Nuclear Technology, Volume 159, pp. 208-220.

Lewis, E.E., Miller, W.F., 1993. Computational Methods of Neutron Transport. American Nuclear Society Publishing, LaGrange Park, IL.

Manalo, K.L., 2008. Development, Optimization, and Testing of a 3-D Zone Based Burnup/Depletion Solver for Deterministic Transport, Master's Thesis. University of Florida, Gainesville, FL.

Mock, T., 2006. Tandem Use of Monte Carlo and Deterministic Methods for Analysis of Large Scale Heterogeneous Radiation Systems, Master's Thesis. University of Florida, Gainesville, FL.

Plower, T.J., 2008. Fully Automated 3-D Parallel Simulation and Optimization of a Full Scale Pressurized Water Reactor Fuel Assembly with Burnup Corrected Cross Sections, Master's Thesis. University of Florida, Gainesville, FL.

Ruddy, F. H., Seidel, J. G., and Dulloo, A.R., 2006. Fast Neutron Dosimetry and Spectrometry using Silicon Carbide Semiconductor Detectors, Journal of ASTM International. Volume 3, No. 3. pp. 408-415.

Sjoden, G.E., 2002. Deterministic adjoint transport applications for He-3 neutron detector design. Annals of Nuclear Energy, Volume 29, pp. 1055-1071.

Sjoden, G.E., Haghighat, A., 2007. The Exponential Directional Weighted (EDW) Differencing Scheme in 3-D Cartesian Geometry. Proceedings of the Joint International Conference on Mathematics and Supercomputing for Nuclear Applications, Saratoga Springs, New York, Vol II, pp.1267-1276.

Sjoden, G.E. Haghighat, A., 2008. PENTRAN^{TM} Code System User Guide to Version 9.4X.1 Series, HSW Technologies, Gainesville, FL.

Williams, M.L., Asgari, M., Hollenbach, D.F., 2006. CENTRM: A One-Dimensional Neutron Transport Code for Computing Pointwise Energy Spectra, SCALE5.1 Manual. Oak Ridge National Laboratory , Oak Ridge, TN

Williams, M.L., Hollenbach, D.F., 2006. PMC: A Program to Produce Multigroup Cross Sections Using Pointwise Energy Spectra from CENTRM, SCALE5.1 Manual. Oak Ridge National Laboratory, Oak Ridge, TN.

BIOGRAPHICAL SKETCH

Mireille Rowe was born in 1985 in Miami, FL and grew up in Panama and Florida. She graduated Charles W. Flanagan in 2003 and began to pursue her degree in the fall of 2003. Mireille was active in the Tau Chapter of Phi Sigma Rho and was also a member of the American Nuclear Society and Alpha Nu Sigma. Mireille received a B.S. in nuclear engineering from the University of Florida in August 2007. She then remained at the University of Florida to receive her M.S. degree in nuclear engineering. Mireille has accepted a job in the nuclear industry and plans to start her career in summer 2009.